Systems/Circuits

NMDA Receptors in the Lateral Preoptic Hypothalamus Are Essential for Sustaining NREM and REM Sleep

Giulia Miracca,[1*] **Berta Anuncibay-Soto,**[1,2*] **Kyoko Tossell,**[1] **Raquel Yustos,**[1] **Alexei L. Vyssotski,**[3] **Nicholas P. Franks,**[1,2] **and William Wisden**[1,2]

[1]Department of Life Sciences, Imperial College London, London SW7 2AZ, United Kingdom, [2]UK Dementia Research Institute, Imperial College London, London SW7 2AZ, United Kingdom, and [3]Institute of Neuroinformatics, University of Zürich/Eidgenössische Technische Hochschule Zürich, Zürich CH-8057, Switzerland

The lateral preoptic (LPO) hypothalamus is a center for NREM and REM sleep induction and NREM sleep homeostasis. Although LPO is needed for NREM sleep, we found that calcium signals were, surprisingly, highest in REM sleep. Furthermore, and equally surprising, NMDA receptors in LPO were the main drivers of excitation. Deleting the NMDA receptor GluN1 subunit from LPO abolished calcium signals in all cells and produced insomnia. Mice of both sexes had highly fragmented NREM sleep-wake patterns and could not generate conventionally classified REM sleep. The sleep phenotype produced by deleting NMDA receptors depended on where in the hypothalamus the receptors were deleted. Deleting receptors from the anterior hypothalamic area (AHA) did not influence sleep-wake states. The sleep fragmentation originated from NMDA receptors on GABA neurons in LPO. Sleep fragmentation could be transiently overcome with sleeping medication (zolpidem) or sedatives (dexmedetomidine; Dex). By contrast, fragmentation persisted under high sleep pressure produced by sleep deprivation (SD), mice had a high propensity to sleep but woke up. By analyzing changes in δ power, sleep homeostasis (also referred to as "sleep drive") remained intact after NMDA receptor ablation. We suggest NMDA glutamate receptor activation stabilizes firing of sleep-on neurons and that mechanisms of sleep maintenance differ from that of the sleep drive itself.

Key words: hypothalamus; NMDA receptor; NREM; preoptic; REM; sleep

---

Significance Statement

Insomnia is a common affliction. Most insomniacs feel that they do not get enough sleep, but in fact, often have good amounts of sleep. Their sleep, however, is fragmented, and sufferers wake up feeling unrefreshed. It is unknown how sleep is maintained once initiated. We find that in mice, NMDA-type glutamate receptors in the hypothalamus are the main drivers of excitation and are required for a range of sleep properties: they are, in fact, needed for both sustained NREM sleep periods, and REM sleep generation. When NMDA receptors are selectively reduced from inhibitory preoptic (PO) neurons, mice have normal total amounts of sleep but high sleep-wake fragmentation, providing a model for studying intractable insomnia.

Introduction

Both NREM and REM sleep are partly controlled by the preoptic (PO) hypothalamus (Nauta, 1946; McGinty and Sterman, 1968; Sherin et al., 1996; John and Kumar, 1998; Lu et al., 2000, 2002;

Szymusiak et al., 2007). In this region, GABA/peptidergic neurons, e.g., GABA/galanin neurons, contribute to NREM sleep induction and sleep homeostasis (Sherin et al., 1996; Zhang et al., 2015; Chung et al., 2017; Kroeger et al., 2018; Ma et al., 2019; Reichert et al., 2019). To stay asleep, it seems reasonable to assume that these sleep-promoting neurons would have to stay "on." Indeed, lesioning of lateral PO (LPO) neurons in rats reduces the amounts of NREM or REM sleep, depending on the location of the lesion (Lu et al., 2000). But molecular factors that keep LPO sleep-promoting neurons firing and so govern the lengths of NREM and REM sleep episodes are not known.

One critical factor maintaining sleep could be NMDA-type glutamate receptors. These channels, especially when located extrasynaptically, can provide tonic excitation (Sah et al., 1989; Papouin et al., 2012; Neupane et al., 2021). Indeed, NMDA receptor activation promotes sleep. In the fruit fly *Drosophila*, genetic knock-down of NMDA receptors in brain reduces total

sleep time (Tomita et al., 2015). In rodents, NMDA receptor antagonists reduce and agonists enhance NREM sleep (Tatsuki et al., 2016; Burgdorf et al., 2019). Furthermore, patients with autoimmunity to the essential GluN1 subunit of NMDA receptors often suffer insomnia (Dalmau et al., 2019; Ariño et al., 2020). Because NMDA receptors are expressed throughout the brain (Moriyoshi et al., 1991; Laurie and Seeburg, 1994; Monyer et al., 1994), these effects on sleep could come from interference with many circuits.

Calcium entry through NMDA receptors has also been suggested to be part of the sleep homeostasis mechanism that tracks time spent awake (Liu et al., 2016). Even if sleep is poor, wakefulness still cannot be sustained beyond a certain limit. This limit is thought to be imposed by the process of sleep homeostasis, the increasing drive to enter NREM sleep as wakefulness continues (Borbély et al., 2016). Sleep homeostasis is operationally studied as an increase in NREM δ power after sleep deprivation (SD; Hanlon et al., 2011; Franken, 2013; Greene et al., 2017; Deboer, 2018). Given that the PO hypothalamus is one of the key regions controlling sleep homeostasis (Zhang et al., 2015; Donlea et al., 2017; Ma et al., 2019; Reichert et al., 2019), we were keen to test how NMDA receptors in the LPO area influence this process.

We found that the whole LPO area has selectively raised calcium activity in REM sleep, and this calcium entry depends on NMDA receptors. In this study we deleted the GluN1 NMDA receptor subunit in the LPO hypothalamus and obtained a marked "insomnia" phenotype with high NREM sleep-wake fragmentation and greatly diminished REM sleep. Sleep homeostasis, however, was unaffected by removing NMDA receptors from LPO. The NREM sleep-wake fragmentation effect is selective for GluN1 expression in GABA neurons.

Materials and Methods
Mice
All experiments were performed in accordance with the United Kingdom Home Office Animal Procedures Act (1986) and were approved by the Imperial College Ethical Review Committee. Wild-type *C57BL/6J* mice were purchased from Charles River at seven/eight weeks of age. *Grin1^{lox}* mice (Tsien et al., 1996) were purchased from The Jackson Laboratory (JAX stock #005246) after kind donation by S. Tonegawa. *Vglut2-Cre* mice (*Vglut2-ires-Cre: Slc17a6^{tm2(cre)Lowl}/J*) and *Vgat-Cre* mice (*Vgat-ires-Cre: Slc32a1^{tm2(cre)Lowl}/J*) were kindly provided by B. B. Lowell and purchased from The Jackson Laboratory (JAX stock #016963 and #016962, respectively; Vong et al., 2011). *Galanin-Cre* mice (*Tg(Gal-cre)KI87Gsat/Mmucd*) were generated by GENSAT and deposited at the Mutant Mouse Regional Resource Center, stock #031060-UCD, GENSAT-Project (NINDS Contracts N01NS02331 and HHSN271200723701C to The Rockefeller University, New York; Schmidt et al., 2013). *Nos1-Cre* mice (*Nos1-ires-Cre^{tm1(cre)Mgmj}/J*), were kindly provided by M. G. Myers, and purchased from The Jackson Laboratory (JAX stock #017526; Leshan et al., 2012).

All mice were housed at a maximum of five mice per cage with food and water *ad libitum* and maintained under the same conditions (21 ± 1°C, reversed 12/12 h light/dark cycle). Zeitgeber time (ZT)0 is defined as the time when the light was switched on (4 P.M.) and ZT12 is defined as the time of light off (4 A.M.). For behavioral experiments, mice were singly housed, and experiments performed during dark phase (ZT12–ZT24) unless otherwise specified, while photometry recordings were performed during light phase (ZT0–ZT12).

Transgenes and AAVs
All AAVs (serotype 1/2) were produced in house. The adenovirus helper plasmid *pFΔ6*, the AAV helper plasmids *pH21* (AAV1) and *pRVI* (AAV2), and the *pAAV* transgene plasmids were co-transfected into HEK293 cells and the resulting AAVs collected on heparin columns, as described previously (Klugmann et al., 2005; Yu et al., 2015). Plasmid

pAAV-iCre-2A-Venus was provided by Thomas Kuner (Abraham et al., 2010). In this *pAAV-iCre-2A-Venus* plasmid, we replaced the original promoter with a small fragment of the mouse histidine decarboxylase (*hdc*) gene basal promoter divorced from cell type-selective enhancers, which we have found this promoter fragment gives strong pan-neuronal expression (promoter sequence and plasmid have been deposited at Addgene, *pAAV-iCre-2A-Venus*: plasmid number 182499, *pAAV-iCre-2A-mCherry*: plasmid number 182246). Plasmid *pAAV-GFP* was a gift from John T. Gray (Addgene plasmid 32396). To create plasmids *pAAV-hsyn-GCaMP6s* and the *pAAV-hsyn-flex-GCaMP6s* (Addgene plasmid 184284), the *GCaMP6s* reading frame from *pGP-CMV-GCaMP6s* (Addgene plasmid 40753, gift of Douglas Kim; T.W. Chen et al., 2013) was mutated into *pAAV-flex-hM3D_q-mCherry* (Krashes et al., 2011), either removing the *flex-hM3D_q-mCherry* component or keeping both sets of *loxP* sites (*pAAV-flex* backbone), respectively. For knocking down GluN1 expression cell type selectively, the pPRIME system (Stegmeier et al., 2005), cloned into AAV transgenes, was used to generate shRNAs (see below, Generation of shRNAs to target GluN1).

Surgeries
All surgeries used adult male and female mice, 8–12 weeks old and were performed under deep general anesthesia with isoflurane (3% induction/2% maintenance) and under sterile conditions. Before starting the surgery, mice were injected subcutaneously with Buprenorphine (Vetergesic 0.3 mg/ml, 1:20 dilution in 0.9% sterile saline solution, final 0.1 mg/kg) and Carprofen (Rimadyl 50 mg/ml, 1:50 dilution in 0.9% sterile saline solution, final 5 mg/kg) and then placed in a stereotaxic frame. Mouse core temperature was constantly checked by rectal probe while respiration rate was regularly checked by eye.

For AAV injections, the virus was injected at a rate of 0.1 μl/min using Hamilton microliter #701 10-μl syringes and a stainless-steel needle (33-gauge, 15 mm long). LPO coordinates used for bilateral injection sites were relative to bregma: AP: +0.40 mm, ML: ±0.75 mm, DV was consecutive, injecting half volume at +5.20 mm and half at +5.15 mm. A total volume of 0.3 μl each side was injected. Control AHA coordinates used for bilateral injections sites were relative to bregma: AP: −0.58 mm, ML: ±0.65 mm, DV: +5.60 mm and +5.50 mm for consecutive injections.

For sleep recordings, EEG screw electrodes were chronically implanted on mice skull and EMG wire electrodes (AS634, Coorner Wire) were inserted in the neck extensor muscles. EEG screws were placed on the skull at (relative to bregma): AP: −1.50 mm, ML: −1.50 mm; AP: −1.50 mm, ML: −2.00 mm; AP: +1.50 mm, ML: −2.00 mm.

For fiber photometry, a monofiber (Ø 200 μm, 0.37 NA, Doric Lenses) was chronically implanted together with EEG and EMG electrodes. The fiber was positioned after AAV injections above the LPO following coordinates relative to bregma: AP: +0.10 mm, ML: −0.90 mm, DV: −5.00 mm.

For all surgeries, the wound was sewed around the head stage and the mouse was left recovering in a heat box. All instrumented mice were single housed to avoid lesions to the head stage. After surgery, mice injected with AAVs were allowed one month for recovering and for the viral transgenes to adequately express before being fitted with Neurologger 2A devices (see below) and undergoing any experimental procedures.

EEG/EMG recordings and analysis
EEG and EMG traces were recorded using Neurologger 2A devices as described previously (Vyssotski et al., 2009; Anisimov et al., 2014; Gelegen et al., 2014), at a sampling rate of 200 Hz. The data obtained from the Neurologger 2A were downloaded and visualized using Spike2 Software (Cambridge Electronic Design). The EEG was high pass filtered (0.5 Hz, −3 dB) using a digital filter, while EMG was band pass filtered between 5 and 45 Hz (−3 dB). To define the vigilance states of Wake, NREM, and REM sleep, δ power (0.5–4.5 Hz) and θ (5–10 Hz) power were calculated, as well as θ:δ power ratio and the EMG integral. Automated sleep scoring was performed using a Spike2 script and the result was manually corrected. For the three vigilance states, percentage amounts were calculate using costume Spike2 scripts.

For sleep architecture analysis, costume MATLAB scripts were used. For stage transitions, we calculated each stage change reported in the hypnogram. The baseline number of transitions for animals lacking NMDA receptors has been represented as percentages over the control group. For sleep-deprived mice, we represented the transition numbers after 6-h SD as a percentage over the baseline value for each animal, in both control and experimental groups. Fast Fourier transformation (512 points) was used to calculate EEG power spectra.

SD protocol and drug testing
Mice were fitted with Neurologger 2A devices and the 24-h sleep-wake baseline (BL) was recorded. After BL, mice with Neurologger 2A devices were sleep deprived from ZT0 for 6 h by introducing novel objects into their home cage (Tobler et al., 1997). To make the procedure minimally stressful, mice were never touched, apart from when changing cages. Sleep recordings were stopped at ZT24(0).

Dexmedetomidine (Dex) injections were prepared from stock solution of 0.5 mg/ml (Dexdomitor), diluted in sterile saline before in jections. Mice were injected (intraperitoneally) with a dose of 25 or 50 µg/kg at ZT21 to record sleep and fragmentation phenotype. Zolpidem injections were prepared by dissolving zolpidem tartrate powder (Sigma-Aldrich) in sterile saline. Mice were injected (intraperitoneally) with 5 mg/kg of solution at ZT23 and their EEG/EMG traces recorded for at least 24 h.

Histology and immunostaining
Animals were perfused transcardially with 20 ml of cold $1\times$ PBS at a rate on 4 ml/min, followed by 20 ml 4% paraformaldehyde (PFA; 4 ml/min) in $1\times$ PBS. Brains were dissected and postfixed in 4% PFA overnight, and then transferred in 30% sucrose. After 3 d in sucrose, brains were cut in 35-µm coronal slice using a microtome (Leica). For staining, slices were transferred in an epitope retrieval solution (0.05% Tween 20, 10 mM sodium citrate buffer, and pH 6.0) for 20 min at 82°C, then left at room temperature (RT) for 15 min before being washed. After three washes of 10 min in $1\times$ PBS, brain slices were blocked in 0.2% Triton X-100 (Sigma-Aldrich), 20% normal goat serum (NGS; Vector Laboratories) in $1\times$ PBS for 1 h at RT, shaking. Primary antibody staining was then performed overnight at 4°C shaking in 0.2% Triton X-100, 2% NGS in $1\times$ PBS. In case of double staining, both primary antibodies were added in the solution unless cross-reactivity was previously observed. The following day, slices were washed three times in $1\times$ PBS for 10 min and then secondary antibody solution was applied for 1 h and 30 min in 0.2% Triton X-100, 2% NGS in $1\times$ PBS, at RT shacking. If double staining was required, washes and another secondary antibody incubation were conducted. After secondary antibodies incubations, slices were washed again for three times for 10 min, RT in $1\times$ PBS shacking and 4′,6-diamidino-2-phenylindole (DAPI) staining (1:5000 in PBS, Hoechst 33 342, Life Technologies) was then performed for a maximum of 10 min. After at least one wash in $1\times$ PBS, slices were ready to be mounted. For mounting, microscope slides (Superfrost PLUS, Thermo Scientific), mounting media ProLong Gold Antifade Reagent (Invitrogen) and glass cover slides (24×50 mm, VWR Internartional) were used. Primary antibodies: rabbit anti-green fluorescent protein (GFP; Invitrogen, A6455, 1:1000), chicken anti-GFP (Abcam, ab13970, 1:1000), rat anti-mCherry (Invitrogen, M11217, 1:1000). Secondary antibodies (all from Invitrogen): Alexa Fluor 488 goat anti-Chicken (A11039, 1:500), Alexa Fluor 488 goat anti-rabbit (A11008, 1:500), Alexa Fluor 594 goat anti rabbit (A11072, 1:500), and Alexa Fluor 568 goat anti-rat (A11077, 1:500).

Acute slice preparation and electrophysiology recordings
Mice were euthanized by cervical dislocation and subsequent decapitation. The brain was rapidly retrieved to be sliced and placed into cold oxygenated NMDG solution (in mM: NMDG 93, HCl 93, KCl 2.5, NaH$_2$PO$_4$ 1.2, NaHCO$_3$ 30, HEPES 20, glucose 25, sodium ascorbate 5, Thiourea 2, sodium pyruvate 3, MgSO$_4$ 10, CaCl$_2$ 0.5). Para-horizontal slices (thickness 300 µm) encompassing the LPO area were obtained using a vibrotome (Vibrating Microtome 7000smz-2; Campden Instruments LTD). Slices were incubated for 15 min in NMDG solution at 33°C with

constant oxygenation and transferred to oxygenated standard aCSF (in mM: NaCl 120, KCl 3.5, NaH$_2$PO$_4$ 1.25, NaHCO$_3$ 25, glucose 10, MgCl$_2$ 1, CaCl$_2$ 2) solution for at least 1 h at RT. Slices were transferred to a submersion recording chamber and were continuously perfused at a rate of 4–5 ml/min with fully oxygenated aCSF at RT. For whole-cell recording, patch pipettes at 4–6 MΩ were pulled from borosilicate glass capillaries (1.5 mm OD, 0.86 mm ID, Harvard Apparatus, #GC150F-10) and filled with intracellular solution containing in mM: 128 CsCH$_3$SO$_3$, 2.8 NaCl, 20 HEPES, 0.4 EGTA, 5 TEA-Cl, 2 Mg-ATP, 0.5 NaGTP (pH 7.35, osmolality 285 mOsm). 0.1% Neurobiotin was included in the intracellular solutions to identify the cell position and morphology following recording. Recordings were performed using a Multiclamp 700B amplifier (Molecular Devices). Access and input resistances were monitored throughout the experiments. The access resistance was typically <20 MΩ, and results we discarded if resistance changed by >20%.

GFP-positive neurons were visually identified and randomly selected. For AMPA and NMDA currents, a bipolar stimulus microelectrode (MX21AEW, FHC) was placed 100–200 µm away caudally from the recording site. The intensity of stimulus (10 ms) was adjusted to evoke a measurable, evoked EPSC in recording cells. AMPA and NMDA mixed currents were measured at a holding potential of +40 mV. After obtaining at least 10 sweeps of stable mixed currents, D-AP5 (50 µM) was perfused in the bath solution for 15 min and AMPA currents were measured. NMDA currents were obtained by subtracting AMPA currents from mixed currents off-line. The peak amplitude of both currents was used for AMDA/NMDA ratio analysis. For spontaneous EPSCs (sEPSCs), GFP-positive LPO neurons were voltage clamped at −70 mV. A stable baseline recording was obtained for 5–10 min. Frequency, amplitude, rise, and decay time constants of sEPSCs were analyzed off-line with the Mini Analysis (Synaptosoft). Frequency was obtained from 2 min of recording. All recordings were made in the presence of picrotoxin (100 µM).

For immunohistochemistry following electrophysiological recordings, brain slices were postfixed in 4% PFA overnight at 4°C. PFA was then washed away three times for 10 min in $1\times$ PBS and slices were blocked and permeabilized in 20% NGS or 2% bovine serum albumin (BSA) for 3-h shaking. Primary anti-GFP antibody to trace viral distribution was diluted in 2% NGS, 0.5/0.7% Triton X-100 in PBS overnight at 4°C shaking. After four washes in $1\times$ PBS for 10 min each, secondary antibody was diluted in 2% NGS and 0.5% Triton X-100 for 3 h at RT and shaking. After washes and to track Neurobiotin-filled neurons recorded by electrophysiology, an Alexa594-conjugated streptavidin (Invitrogen) was diluted 1:500 in 1% NGS, 0.5% Triton X-100 and slices were incubated for 2–3 h at RT. Four washes of 15 min and subsequent DAPI incubation for 10 min were performed before slices were mounted on glass slides.

Calcium photometry
Following four weeks of recovery, mice were acclimatized to the testing environment for at least 2 h before behavioral experiments and then recorded for 6 h during the light period. The light source was a 473 nM diode-pumped solid state (DPSS) laser with fiber coupler (Shanghai Laser & Optics century Co) and adjustable power supply (Shanghai Laser & Optics century Co), controlled by a Grass SD9 stimulator. A lock-in amplifier (SR810, Stanford Research Systems) was used to drive the laser at 125-Hz TTL pulses with an average power of 80 µW at the tip of the fiber directly connected to the mouse. The light source was coupled to a fluorescence cube (FMC_GFP_FC, Doric Lenses) through an optical fiber patch cord (Ø 200 µm, 0.22 NA, Doric Lenses). From the filter cube, an optical patch cord (Ø 200 µm, 0.37 NA, Doric Lenses) was connected to the monofiber chronically implanted in the mouse brain using ceramic sleeves (Thorlabs). The GCaMP6s output was then filtered at 500–550 nm through the fluorescence cube, converted to a voltage by a photodiode (APD-FC, Doric Lenses) and then amplified by the lock-in amplifier with a time constant of 30 ms. Finally, the signal was digitalized using a CED 1401 Micro box (Cambridge Electronic Design) and recorded at 200 Hz using Spike2 software (Cambridge Electronic Design). Photometry, EEG and EMG data were aligned offline using

Spike2 software and analyzed using custom MATLAB (MathWorks) scripts. For each experiment, the photometry signal F was normalized to baseline using the function $\Delta F/F = (F-F_0)/F_0$, where F_0 is the mean fluorescence across the signal analyzed. When scatter plots of $\Delta F/F$ levels were plotted for each behavioral state, $\Delta F/F$ values were obtained by calculating the average F over a 50-s rolling window, with a 0.2-Hz sampling rate over 70–90 min of photometry recordings. We applied a custom MATLAB script to correct the baseline photometry values for photobleaching and photometry signal drift during long recordings.

Generation of shRNAs to target GluN1

We used the Potent RNA Interference using MicroRNA Expression (PRIME) system, where shRNAs are placed into the context of a mir30 miRNA sequence (Stegmeier et al., 2005). By consulting the website http://katahdin.cshl.org, three shRNAs were designed to target exons 11–18 of the *Grin1* gene, encoding the region from amino acids 409–683 of GluN1. The sequences were amplified from mouse genomic DNA using primers (pSM2C forward: 5′-GATGGCTG-CTCGAG-AAGGTATAT-TGCTGTTGACAGTGAGCG-3′; pSM2C reverse: 5′-GTCTAGAG-GAATTC-CGAGGCAGTAGGCA-3′), following the protocol previously described (Stegmeier et al., 2005).

The three sequences were referred to as shRNA-GluN1-1.1, -2, or -3 (the underlined sequences are the 22-mers specific for the GluN1 subunit):

shRNA-GluN1.1 targeted the GluN1 sequence at 1800 bp (600 aa) of the coding sequence: 3′-TGCTGTTGACAGTGAGCGAACTGACCCTGTCCTCTGCCATTAGTGAAGCCACAGATGTAA<u>TGGCAGAGGA</u>CAGGGTCAGTGTGCCTACTGCCTCGGA-5′;

shRNA-GluN1.2 targeted the GluN1 sequence from 2565 bp (855 aa) of the coding sequence: 3′-TGCTGTTGACAGTGAGCGCGCCGTGAACGTGTGGAGGAAGTAGTGAAGCCACAGATGTAC<u>TTCCTCCAC</u>ACGTTCACGGCTTGCCTACTGCCTCGGA-5′;

shRNA-GluN1.3 targeted the GluN1 sequence at 2215 bp (738 aa) of the coding region: 3′-TGCTGTTGACAGTGAGCG<u>CGGAGTTTGA</u>GGCTTCACAGAATAGTGAAGCCACAGATGTA<u>TTCTGTGAAGCC</u>TCAAACTCCATGCCTACTGCCTCGGA-5′;

As a control for shRNA-GluN1 sequences, an shRNA scramble hairpin was used, not complementary to sequences in the mouse genome. The shRNA-scramble (scr) sequence was:

3′-GCTGTTGACAGTGAGCGAGCTCCCTGAATTGGAATCCTAGTGAAGCCACAGATGTAGGATTCCAATTCAGCGGGAGCCTGCCTACTGCCTCGGA-5′.

The three *shRNA-GluN1* hairpins and the *shRNA-scr* hairpin were cloned into the *pPRIME* vector to be then expressed and tested in HEK293 cells. To establish shRNA efficiencies in knocking down the NMDA GluN1 subunit expression, a plasmid was constructed expressing *GluN1-2A-mCherry* under the control of the CMV promoter. Each *GluN1-shRNA pPRIME* plasmid was then transfected into HEK293 cells together with *pGluN1-2A-mCherry*. After 60 h in culture, mCherry fluorescence was quantified. The GluN1.3 shRNA produced lower fluorescence intensity, and thus higher inhibition of GluN1 expression, and it was therefore cloned into an AAV transgene cassette in an inverse orientation flanked by lox sites, as we described previously (Yu et al., 2015), to produce *pAAV-flex-GFP-shRNA-GluN1* with an *hdc* promoter fragment (this plasmid has been deposited at Addgene, number 182502) which was then packaged into AAV capsids (as above). The AAV transgene expresses GFP as well as shRNA-GluN1. For the controls, we packaged *pAAV-flex-GFP-shRNA*-scramble (this plasmid has been deposited at Addgene, number 182503).

Experimental design and statistical analysis

Origin, MATLAB and GraphPad Prism 8 were used for graphs and statistical analysis. Data collection and experimental procedure conditions were randomized. The experimenter was not blinded during the procedures. Data are presented as mean ± SEM. The normality of each dataset distribution was tested using the Kolmogorov–Smirnoff test. Paired/unpaired two-tailed Student's t test or one-way ANOVA were used to compare groups when only one variable was present. For longitudinal measurements, or measurements with two separate independent

variables, a two-way repeated measures ANOVA, or a simple two-way ANOVA followed by *post hoc* Sidak's, Tukey's, or Dunnett's tests were performed. F and p values reported in the text are relative to the ANOVA statistical tests. Significantly different time points obtained through a multiple comparison analysis in the context of a two-way ANOVA test are indicated in the figures, where $*p < 0.05$, $**p < 0.005$, $***p < 0.0005$, $†p < 0.00005$. When the data were not normally distributed, a Mann–Whitney test was performed. Statistical significance was considered when $*p < 0.05$, $**p < 0.005$, $***p < 0.0005$.

Results

Activity in LPO neurons is highest during REM sleep

We first recorded neuronal activity in all LPO neurons using photometry with the calcium sensor GCaMP6s. Mice were injected in LPO with *AAV-GCaMP6s* (Fig. 1A,B). The highest calcium activity occurred during REM sleep episodes, especially at the beginning and end of the episodes (Fig. 1C,D). During NREM sleep, LPO neurons showed a more sporadic and spiky activity, and during wakefulness only low activity. By plotting scaled means of the GCaMP6s signal against EMG signal (Fig. 1E, left panel) and δ power (Fig. 1E, center panel), REM sleep episodes were distributed toward higher values of GCaMP6s signal, separating them from the NREM sleep and Wake data points. Comparing the average of $\Delta F/F$ points during each behavioral state, REM sleep calcium values were significantly higher than in other vigilance states (one-way ANOVA: $F_{(2,21)} = 4.47$, $p = 0.02$; Tukey's *post hoc* test: Wake vs NREM sleep $p = 0.75$, Wake vs REM sleep $p = 0.10$, NREM vs REM sleep $p = 0.02$, $n = 8$; Fig. 1E, right panel).

Photometry recordings were also performed in subtypes of LPO neurons by injecting *AAV-flex-GCaMP6s* into the LPO area of *Vgat-Cre*, *Vglut2-Cre*, *Nos1-Cre*, and *Galanin-Cre* mice (Fig. 1F). As for the pan-neuronal recordings, these subsets all showed a significantly higher activity during REM sleep episodes compared with NREM sleep and Wake (*Vgat-Cre*: one-way ANOVA: $F_{(2,12)} = 16.87$, $p = 0.0003$, Tukey's *post hoc* test: Wake vs NREM sleep $p = 0.79$, Wake vs REM sleep $p = 0.0005$, NREM vs REM sleep $p = 0.001$, $n = 5$, *Vglut2-Cre*: one-way ANOVA: $F_{(2,12)} = 26.94$, $p < 0.0001$, Tukey's *post hoc* test: Wake vs NREM sleep $p = 0.3$, Wake vs REM sleep $p = 0.0003$, NREM vs REM sleep $p < 0.0001$, $n = 5$, *NOS1-Cre*: one-way ANOVA: $F_{(2,12)} = 15.82$, $p = 0.0004$, Tukey's *post hoc* test: Wake vs NREM sleep $p = 1.00$, Wake vs REM sleep $p = 0.001$, NREM vs REM sleep $p = 0.001$, $n = 5$, *Galanin-Cre*: one-way ANOVA: $F_{(2,12)} = 21.55$, $p = 0.0001$, Tukey's *post hoc* test: Wake vs NREM sleep $p = 0.28$, Wake vs REM sleep $p = 0.0001$, NREM vs REM sleep $p = 0.001$, $n = 5$; Fig. 1F).

Deletion of NMDA receptors from LPO neurons abolishes neuronal activity

NMDA receptors assemble as heteromeric tetramers of subunits, with two core GluN1 subunits, whose gene, *grin1*, is transcribed throughout the brain (Moriyoshi et al., 1991), and GluN2 and/or GluN3 subunits, whose genes are differentially expressed (Monyer et al., 1992, 1994; Laurie and Seeburg, 1994; Paoletti et al., 2013; Tovar et al., 2013). GluN1 is essential for all NMDA receptors (Tsien et al., 1996; Paoletti et al., 2013). Mice homozygous for a conditional allele ($Grin1^{lox}$) that encodes the GluN1 subunit were bilaterally injected into the LPO with *AAV-iCre-2A-Venus*, generating $\Delta GluN1$-*LPO* mice (Fig. 2A). Histologic analysis confirmed that the *AAV-iCre-2A-Venus* transgene expression was restricted to the LPO
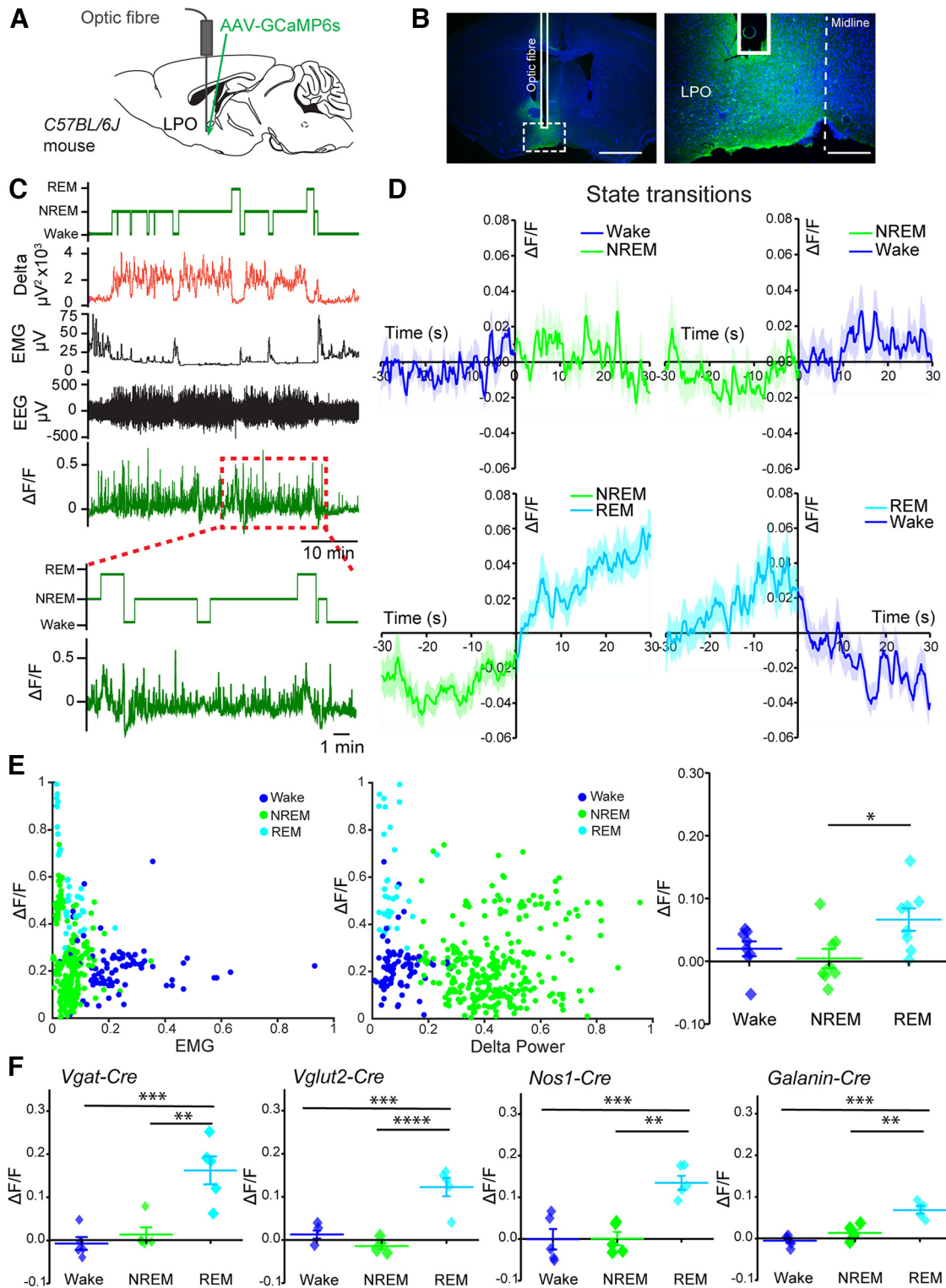
Figure 1. Activity in LPO hypothalamic neurons is highest during REM sleep. ***A***, Schematic representation of optic fiber implantation and *AAV-GCaMP6s* injection in LPO area of *C57BL/6J* mice. ***B***, Immunohistochemistry staining showing viral vector expression in LPO, using GFP (in green) antisera and DAPI (in blue). The optic fiber tract is also shown. Scale bars: 1 mm (left) and 200 μm (right). ***C***, Example of photometry recording from LPO neurons aligned to EEG and EMG data. From the top: stage, δ power, EMG, EEG, and $\Delta F/F$ from GCaMP6s signal corrected for baseline drift. The dotted red square indicates the segment of the trace expanded below. ***D***, Photometry recordings across state transitions normalized as $\Delta F/F$ data points (mean $\pm$ SEM). For the transitions to be considered, animals had to be in the behavioral state before and after transitions for at least 30 s each. ***E,*** Left and center panels, Scaled $\Delta F/F$ signal plotted against EMG (left) and δ power (right). Right panel, Quantification of LPO calcium activity as $\Delta F/F$ by behavioral state. ***F***, Screening of LPO neuronal populations for calcium activity shown as $\Delta F/F$ using gene-specific Cre mouse lines (*Vgat-Cre, Vglut2-Cre, Nos1-Cre, Galanin-Cre*) and injection of *AAV-flex-GCaMP6s*. Data are mean $\pm$ SEM (*$p < 0.05$, **$p < 0.005$, ***$p < 0.0005$).
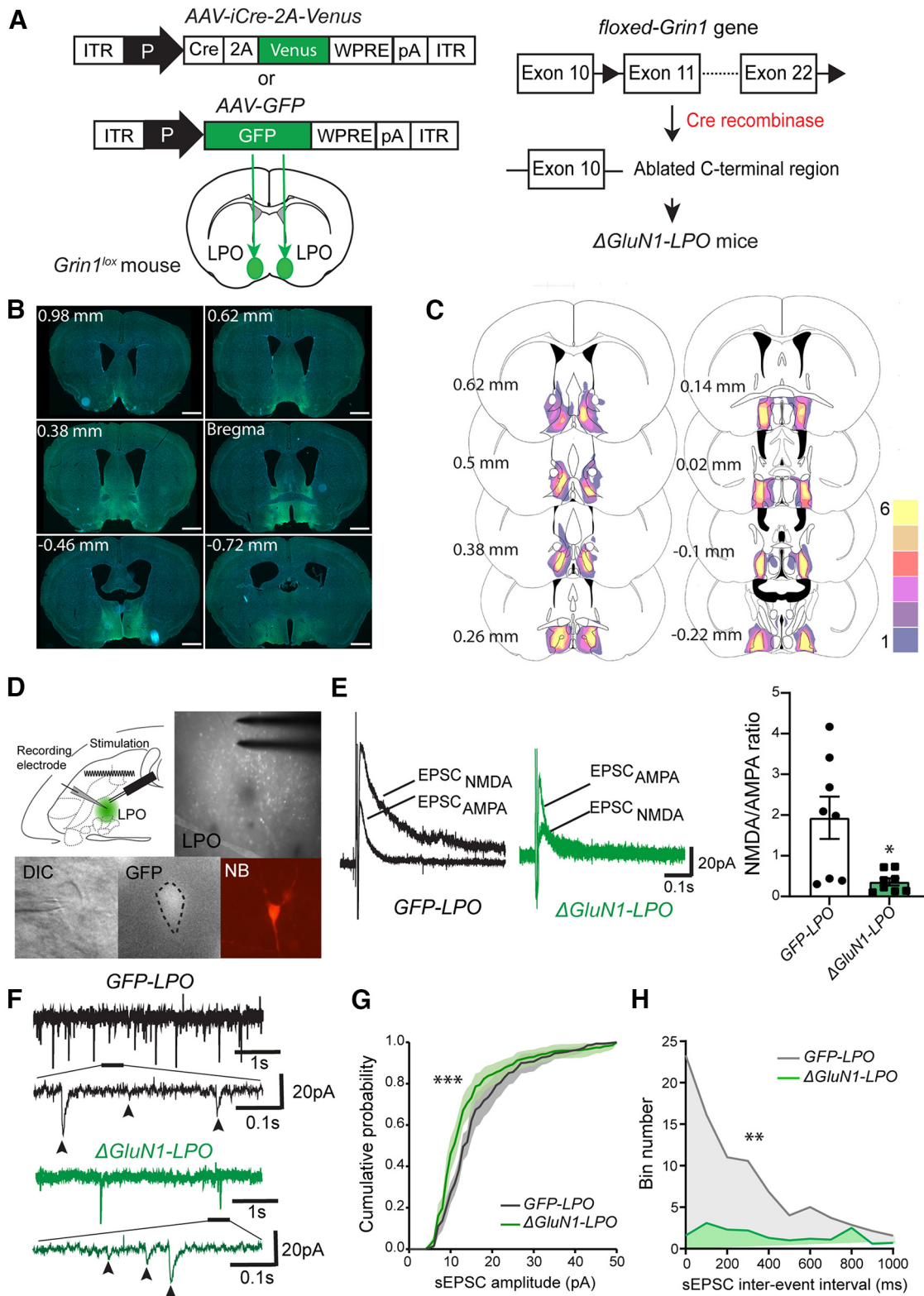
Figure 2. *AAV-Cre-Venus* mapping and characterization of EPSCs in Δ*GluN1-LPO* mice. *A*, Generation of Δ*GluN1-LPO* and *GFP-LPO* animals by bilateral injection in LPO of *AAV-Cre-2A-Venus* and *AAV-GFP*, respectively. In *Grin1^{lox}* mice, the C-terminal region of the *Grin1* gene is flanked by loxP sites (black arrowheads). When the Cre recombinase is expressed, it permanently excises the region between the loxP sites, and the *grin1* gene no longer encodes a functional NR1 subunit. Without the NR1 subunit, NMDA receptors cannot form. *B*, Mapping of Cre recombinase expression using immunohistochemistry (iCre-2A-Venus in green; DAPI in blue). Coordinates are relative to bregma. Scale bars: 1 mm. *C*, Schematic representation of viral injection area and expression of the *AAV-Cre-2A-Venus* transgene (Δ*GluN1-LPO*, n = 6). In the heat map, yellow corresponds to areas were all six mice showed Venus-expressing cells as detected by immunohistochemistry, whereas dark purple indicates areas where only one mouse showed Venus-positive cells. Coordinates are relative to bregma. *D*, Top left, Schematic of para-horizontal *ex vivo* brain slice showing the positioning of stimulus matrix and recording electrode. Top right, Microscope images of GFP+ (Venus-positive) cells transduced with *AAV-iCre-2A-Venus* in LPO with stimulus electrode in sight. The cell successfully patched is shown in differential interface contrast (DIC), gray-scale for GFP and Neurobiotin (NB) immune-detection (left to right, bottom row). *E*, Left panel, Example traces of NMDA receptor-mediated and AMPA receptor-mediated currents (labeled as EPSC_NMDA and EPSC_AMPA, respectively) in *GFP-LPO* (in black) and Δ*GluN1-LPO* (in green)

area, with no spreading toward the medial PO or septal areas ($n = 6$; Fig. 2B,C).

We examined whether NMDA-receptor currents were deleted from $\Delta GluN1$-LPO neurons compared with control *GFP-LPO* mice injected with *AAV-GFP* by recording evoked eEPSCs from *ex vivo* acute slices prepared from the PO area (Fig. 2D,E). Both NMDA receptor-mediated slow currents (hundreds of milliseconds) and AMPA receptor-mediated fast currents (few milliseconds) were found on LPO neurons of *GFP-LPO* mice. NMDA receptor-mediated currents were smaller and the NMDA/AMPA ratio was significantly reduced in cells from $\Delta GluN1$-LPO mice [two-tailed Mann–Whitney test, $U = 10$, $p = 0.02$. $\Delta GluN1$-LPO ($n = 8$); $n = 5$; Fig. 2E].

We also observed sEPSCs (Fig. 2F) and quantified their amplitude and frequencies in both experimental groups. As seen from the cumulative probability histogram of sEPSC amplitude, deletion of the NMDA receptor-mediated current from LPO neurons also reduced spontaneous sEPSCs amplitudes (two-way ANOVA and Sidak's *post hoc* test: "probability," $F_{(50,765)} = 130$, $p < 0.0001$; "virus": $F_{(1,765)} = 25$, $p < 0.0001$; Fig. 2G); and from determining the cumulative bin number of interinterval events (IEIs) of sEPSCs, the frequency of excitatory events was also reduced (two-way ANOVA and Sidak's *post hoc* test: "probability," $F_{(25,390)} = 3.1$; "virus": $F_{(1,390)} = 15.3$, $p < 0.005$; Fig. 2H).

We next tested how NMDA receptor deletion from LPO neurons influenced intracellular calcium transients. We co-injected into the LPO area of *Grin1^{lox}* mice *AAV-iCre-2A-mCherry* and *AAV-flex-GCaMP6s*, so that only neurons expressing Cre recombinase expressed the calcium sensor (Fig. 3A). Regardless of vigilance state, calcium activity in $\Delta GluN1$-LPO neurons was greatly reduced; indeed, no calcium fluctuations or variation from the baseline levels were observed during any of the three vigilance states in $\Delta GluN1$-LPO neurons (one-way ANOVA: $F_{(2,27)} = 0.69$, $p = 0.51$; Tukey's *post hoc* test: Wake vs NREM sleep $p = 0.54$, Wake vs REM sleep $p = 0.60$, NREM vs REM sleep $p = 0.99$ $n = 5$; Fig. 3B,C), and REM sleep was no longer highlighted by calcium activity, showing that deleting NMDA receptors ablates calcium fluctuations from LPO neurons.

Deletion of NMDA receptors from LPO neurons reduces NREM and REM sleep and produces high sleep-wake fragmentation

We examined the effect on vigilance states of deleting GluN1 from LPO neurons (Fig. 4A,B). Over 24 h, $\Delta GluN1$-LPO mice compared with *GFP-LPO* mice spent more time awake (two-way repeated measures ANOVA and Sidak's *post hoc* test: Wake time, $F_{(8.6,181)} = 14$, $p < 0.0001$; NREM sleep time, $F_{(9,188)} = 12.7$, $p < 0.0001$; virus type, $F_{(1,21)} = 41$, $p < 0.0001$; REM sleep time: $F_{(9,190)} = 8.3$, $p < 0.0001$; virus type, $F_{(1,21)} = 18$, $p = 0.0004$; $\Delta GluN1$-LPO, $n = 11$; *GFP-LPO*, $n = 12$; Fig. 4C). $\Delta GluN1$-LPO mice lost on average 15–20% of NREM sleep time and 50% of their REM sleep time during both light and dark periods when compared with controls (two-way ANOVA and Sidak's *post hoc*

test: light phase, vigilance state, $F_{(2,63)} = 795$, $p = 0.0001$; virus type, $F_{(1,63)} = 0.0003$, $p = 0.98$; dark phase, vigilance state, $F_{(2,63)} = 957$, $p < 0.0001$; virus type, $F_{(1,63)} = 0.00001$, $p = 1$; $\Delta GluN1$-LPO, $n = 11$; *GFP-LPO*, $n = 12$; Fig. 4D). EEG power spectra for Wake and NREM sleep were similar between control and $\Delta GluN1$-LPO mice (two-way ANOVA and Sidak's *post hoc* test: Wake frequency, $F_{(89,1800)} = 746$, $p < 0.0001$; virus type, $F_{(1,1800)} = 9.1 \times 10^{-9}$, $p = 1$; NREM sleep frequency: $F_{(89,1800)} = 1601$, $p < 0.0001$; virus type, $F_{(1,1800)} = 1.4 \times 10^{-8}$, $p = 1$; REM sleep frequency, $F_{(89,1800)} = 399$, $p < 0.0001$; virus type, $F_{(1,1800)} = 4.2 \times 10^{-9}$, $p = 1$; $n = 11$; *GFP-LPO*, $n = 12$; Fig. 4E); however, $\Delta GluN1$-LPO mice had strongly reduced cortical θ oscillations during REM sleep episodes (5–10 Hz; Fig. 4E, right panel). Consequently, EEG and EMG recordings during REM sleep episodes showed a reduced θ:δ power (T:D) ratio in $\Delta GluN1$-LPO mice compared with controls (unpaired two-tailed Student's t test, $t = 6.076$, df = 50, $p < 0.0005$; *GFP-LPO*, $n = 7$; $\Delta GluN1$-LPO, $n = 7$; Fig. 4F), although muscle atonia, the other hallmark of REM sleep, was maintained in both groups (Fig. 4G). To verify this, we plotted raw EMG values during REM sleep episodes, finding no differences between the experimental groups (two-way ANOVA and Sidak's *post hoc* test: interaction, $F_{(24,1200)} = 0.15$, $p > 0.99$; time, $F_{(24,1200)} = 0.18$, $p > 0.99$; group, $F_{(1,1200)} = 0.15$, $p = 0.7$. $\Delta GluN1$-LPO, $n = 5$; *GFP-LPO*, $n = 5$; 5 episodes per animal; Fig. 4H).

In addition to sleep loss and reduced cortical θ power, $\Delta GluN1$-LPO mice had a highly fragmented sleep-wake phenotype: they lacked long Wake and NREM sleep episodes, as they had significantly more Wake and NREM sleep episodes (two-way ANOVA and Sidak's *post hoc* test: vigilance state, $F_{(5,126)} = 232$, $p < 0.0001$; virus type, $F_{(1,126)} = 122$, $p < 0.0001$; $\Delta GluN1$-LPO, $n = 11$; *GFP-LPO*, $n = 12$ mice; Fig. 4I, left panel), with a decrease in their mean duration (two-way ANOVA and Sidak's *post hoc* test: vigilance state, $F_{(5,126)} = 60.36$, $p < 0.0001$; virus type, $F_{(1,126)} = 105$, $p = 0.0001$; $\Delta GluN1$-LPO, $n = 11$; *GFP-LPO*, $n = 12$; Fig. 4I, center panel). Indeed, removing the NMDA receptor from LPO neurons increased transitions between wake to NREM sleep by >55% and NREM sleep to wake by >80% during both light and dark period (unpaired two-tailed Student's t test, for the light phase: Wake → NREM, $\Delta GluN1$-LPO = 213 ± 10, *GFP-LPO* = 131 ± 4 transitions, $t = 7.410$, df = 21, $p < 0.0005$; NREM → Wake, $\Delta GluN1$-LPO = 194 ± 10, *GFP-LPO* = 105 ± 6 transitions, $t = 7.346$, df = 21, $p < 0.0005$; for dark phase: Wake → NREM, $\Delta GluN1$-LPO = 179 ± 11, *GFP-LPO* = 116 ± 7 transitions, $t = 4.839$, df = 21, $p < 0.0005$; NREM → Wake, $\Delta GluN1$-LPO = 171 ± 11, *GFP-LPO* = 102 ± 7 transitions, $t = 5.261$, df = 21, $p < 0.0005$, Fig. 4I, right panel). For REM sleep in $\Delta GluN1$-LPO mice, there was a decrease in episodes number, in episodes durations and in transitions to and from this vigilance state (unpaired two-tailed Student's t test, for the light phase, NREM→ REM and REM → Wake, $\Delta GluN1$-LPO = 19 ± 3, *GFP-LPO* = 27 ± 2 transitions, $t = 1.961$, df = 21, $p = 0.06$; for the dark phase, NREM→ REM and REM → Wake, $\Delta GluN1$-LPO = 8 ± 2, *GFP-LPO* = 14 ± 1 transitions, $t = 2.741$, df = 21, $p = 0.012$; Fig. 4I).

Hypothalamic region-specific effect of NMDA receptor ablation on sleep-wake fragmentation

As a control, we tested whether deleting NMDA receptors in a region neighboring the PO area, the anterior hypothalamic area (AHA), caused sleep loss or fragmentation. Bilateral injection of *AAV-iCre-2A-Venus* and *AAV-GFP* into the AHA of *Grin1^{lox}* mice, to generate $\Delta GluN1$-AHA and *GFP-AHA*

←

cells. Right panel, NMDA/AMPA ratios from *GFP-LPO* and $\Delta GluN1$-LPO neurons showing a reduction of NMDA currents in $\Delta GluN1$-LPO neurons. **F,** Example of sEPSC recording from *GFP-LPO* (top, in gray) and $\Delta GluN1$-LPO (bottom, in green) neurons. Part of each recording has been magnified to show the raw sEPSCs; currents are further indicated by arrowheads. **G,** Cumulative probability histogram of sEPSCs amplitude. **H,** Cumulative bin number of IEIs of sEPSCs. Data are mean ± SEM (*$p < 0.05$, **$p < 0.005$, ***$p < 0.0005$).
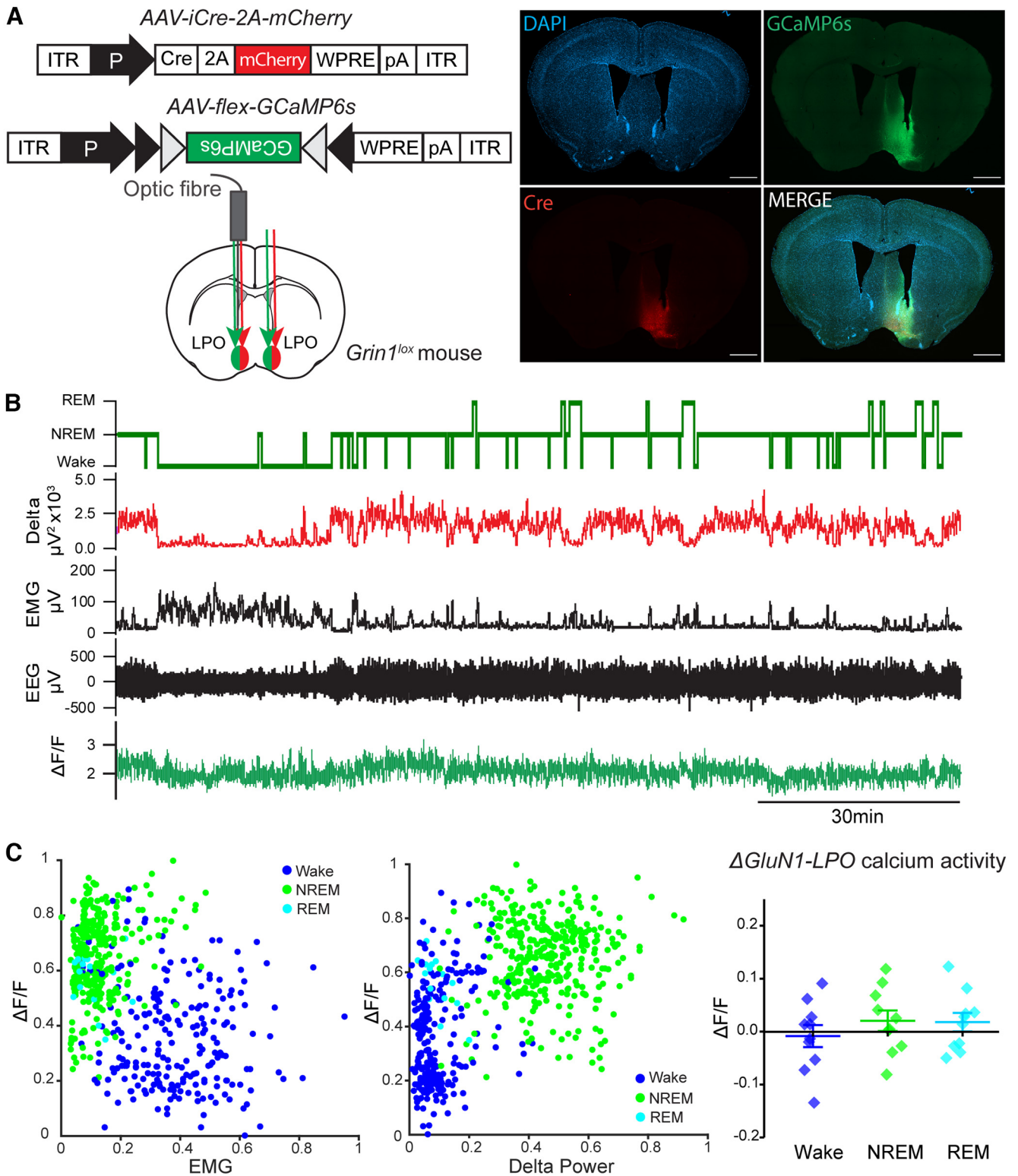
Figure 3. Activity in LPO hypothalamic neurons requires NMDA receptors. **A**, *Grin1^lox* mice were bilaterally co-injected in LPO with *AAV-iCre-2A-mCherry* and *AAV-flex-GCaMP6s* to record calcium levels from neurons lacking NMDA receptors. An optic fiber was also implanted unilaterally for these recordings. Right, Immunohistochemistry showing from left to right: DAPI (blue) and *AAV-flex-GCaMP6s* transgene (green) on the first row, Cre recombinase (red) and merge on the second row. Scale bars: 1 mm. **B**, Example of a photometry recording aligned to EEG and EMG in a *ΔGluN1-LPO* mouse. From the top, Vigilance state, δ power, EMG, EEG, and $\Delta F/F$ from GCaMP6s signal corrected for baseline drift. **C**, Left and center panels, Scaled $\Delta F/F$ GCaMP6s signal plotted against EMG (left) and δ power (center). Right panel, Quantification of *ΔGluN1-LPO* calcium activity normalized as $\Delta F/F$ during behavioral states. Data in the right panel are mean $\pm$ SEM.

mice, respectively (Fig. 5A,B) did not affect sleep and wake amounts during either the light or dark phases (two-way ANOVA and *post hoc* Sidak's test: light phase, virus type, $F_{(1,21)} = 5.4 \times 10^{-6}$, $p = 1$; vigilance state, $F_{(2,21)} = 321$, $p < 0.0001$. During dark phase, virus type, $F_{(1,21)} = 1.9 \times 10^{-6}$, $p = 1$; vigilance state, $F_{(2,21)} = 328$, $p < 0.0001$; Fig. 5C, left and center panels). Nor did the deletion influence the number of transitions between vigilance states (unpaired two-tailed Student's *t* test, NREM → Wake, *ΔGluN1-*
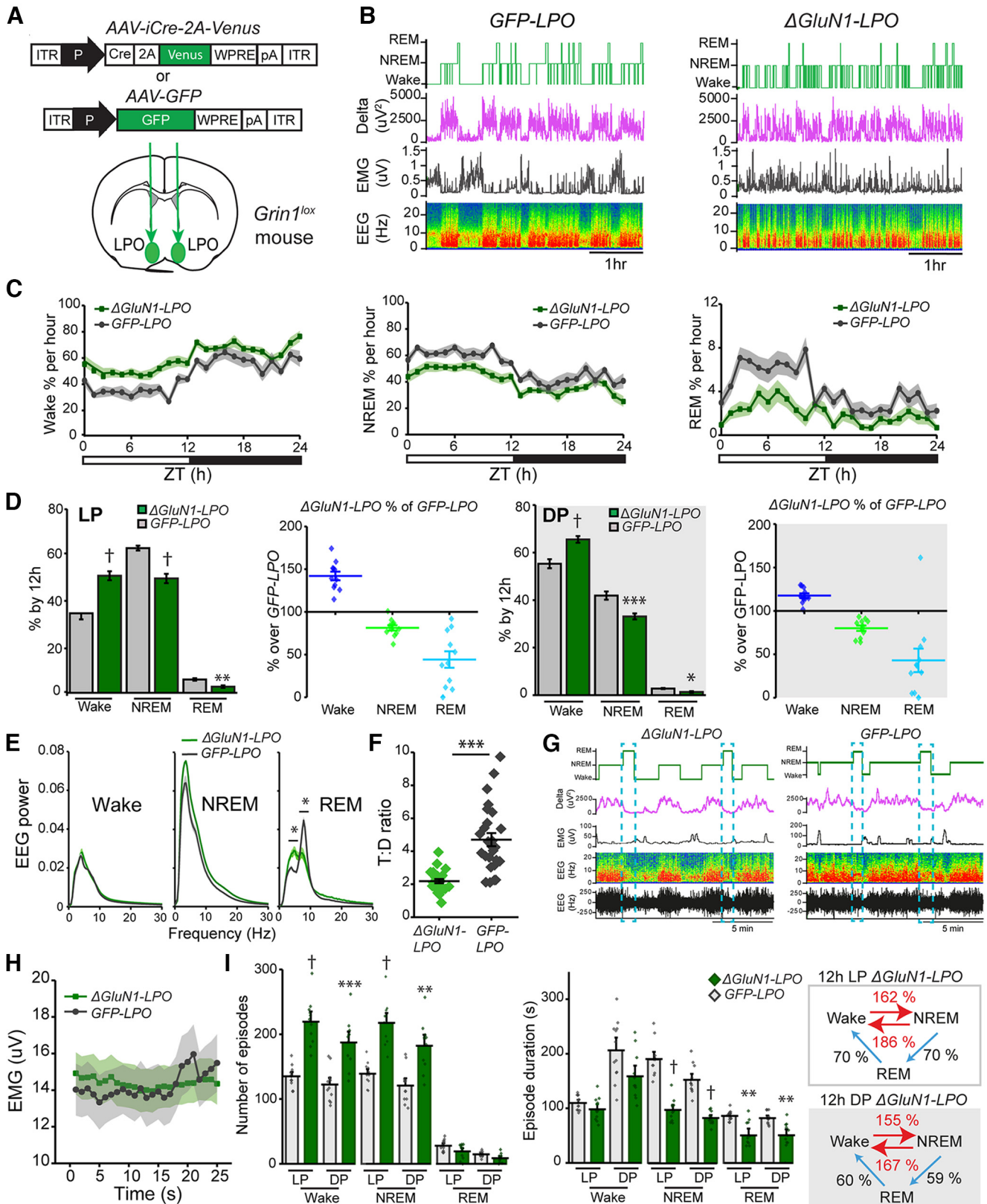
Figure 4. Deletion of NMDA receptors in LPO reduces NREM and REM sleep time and produces sleep-wake fragmentation. **A**, Bilateral *AAV-iCre-2A-Venus* and *AAV-GFP* virus injections into LPO of *Grin1^lox^* mice to generate ΔGluN1-LPO and GFP-LPO control mice, respectively. **B**, Example baseline recordings from GFP-LPO (left) and ΔGluN1-LPO (right) mice. From the top, hypnogram, δ power, EMG, and EEG represented as a somnogram and as a trace. **C**, Twenty-four-hour baseline states distribution as percentage of 1 h of wake (left), NREM (center), and REM sleep (right) during light period (LP: ZT0–ZT12) and dark period (DP: ZT12–ZT24). **D**, First and third panels, quantification of each behavioral state as percentage over LP (first panel) and DP (third panel). Second and fourth panels, Wake, NREM, and REM sleep amounts in ΔGluN1-LPO mice represented as percentage of GFP-LPO mice amounts during LP (second panel) and DP (fourth panel). **E**, EEG power spectrum for Wake (left), NREM (center), and REM sleep (right) normalized over total EEG power. **F**, Quantification of the θ:δ (T:D) ratio in ΔGluN1-LPO and GFP-LPO mice. Each point represents a 100-s average of the T:D ratio during three REM episodes per animal. **G**, Example baseline recordings showing EMG signal (atonia) during REM sleep bouts in

$AHA = 232 \pm 34$, $GFP\text{-}AHA = 254 \pm 42$ transitions, $t = 0.4110$, $df = 7$, $p = 0.7$; Wake $\rightarrow$ NREM, $\Delta GluN1\text{-}AHA = 274 \pm 32$, $GFP\text{-}AHA = 299 \pm 41$ transitions, $t = 0.4757$, $df = 7$, $p = 0.6$; NREM $\rightarrow$ REM and REM $\rightarrow$ Wake, $\Delta GluN1\text{-}AHA = 43 \pm 4$, $GFP\text{-}AHA = 45 \pm 2$ transitions, $t = 0.4175$, $df = 7$, $p = 0.7$; Fig. 5C, right panel). $\Delta GluN1\text{-}AHA$ mice did not show sleep fragmentation: the episode number of NREM and REM sleep epochs and their mean duration were similar to $GFP\text{-}AHA$ mice (two-way ANOVA and post hoc Sidak's test left panel, during light phase, virus type, $F_{(1,21)} = 1.4$, $p = 0.2$; vigilance state, $F_{(2,21)} = 27$, $p < 0.0001$; during dark phase, virus type, $F_{(1,21)} = 0.1$, $p = 0.1$; vigilance state, $F_{(2,21)} = 86$, $p < 0.0001$; right panel during light phase, virus type $F_{(1,21)} = 1$, $p = 0.3$; vigilance state, $F_{(2,21)} = 11$, $p < 0.0001$; during the dark phase, virus type, $F_{(1,21)} = 0.03$, $p = 0.9$; vigilance state, $F_{(2,21)} = 24$, $p < 0.0001$; $GFP\text{-}AHA$, $n = 4$, $\Delta GluN1\text{-}AHA$, $n = 5$; Fig. 5D). Therefore, the fragmented sleep phenotype produced by deleting NMDA receptors originates region selectively in the PO hypothalamus.

The insomnia of mice with NMDA receptors deleted from the LPO hypothalamus persists under high sleep pressure

In both fruit flies and mice, calcium entry through NMDA-type ionotropic glutamate-gated receptors has been proposed to signal the sleep homeostatic process (Liu et al., 2016; Tatsuki et al., 2016; Raccuglia et al., 2019). To investigate whether the fragmented sleep of $\Delta GluN1\text{-}LPO$ mice persisted under high sleep pressure and whether NMDA receptors in LPO were required for sleep homeostasis, we performed 6 h of SD at the onset of the "lights on" period (ZT0) when the sleep drive is highest (Fig. 6A). Although $\Delta GluN1\text{-}LPO$ mice were awake and moving during the SD, there were several indications that they were under high sleep pressure. During the SD, the EEG θ power in $\Delta GluN1\text{-}LPO$ mice was greatly reduced (Fig. 6B, red trace, when compared with $GFP\text{-}LPO$ mice), and most of the power was concentrated in the δ frequency band (two-way ANOVA and Sidak's post hoc test: EEG frequency,
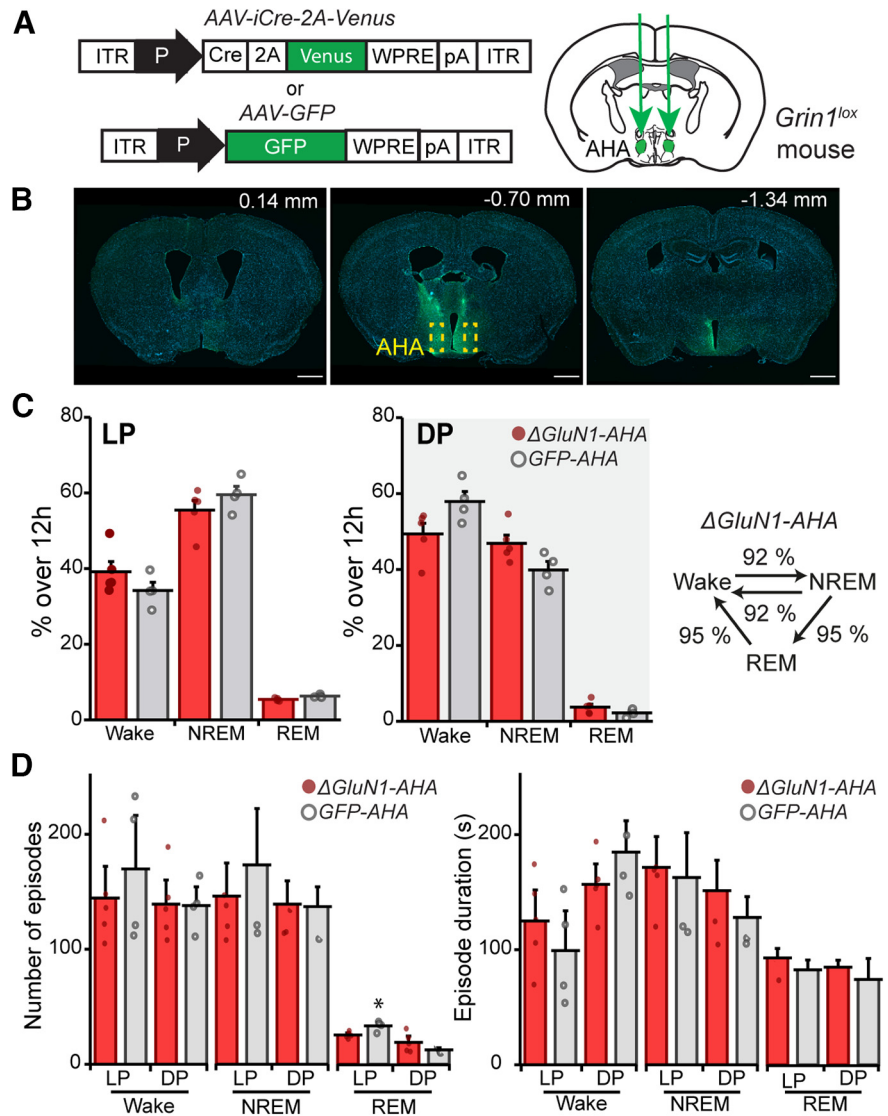

Figure 5. Deletion of the NR1 NMDA receptor subunit in the AHA does not alter sleep-wake states. **A**, AAV-iCre-2A-Venus or AAV-GFP bilateral injection in the AHA to generate $\Delta GluN1\text{-}AHA$ and $GFP\text{-}AHA$ mice. **B**, Viral distribution from LPO to mid-thalamus, the AHA is indicated by the dashed yellow squares. Scale bars: 1 mm. **C**, Baseline state distribution shown as a percentage over 12 h during light phase (LP) left panel, and dark phase (DP) center panel, comparing $\Delta GluN1\text{-}AHA$ with $GFP\text{-}AHA$ mice, right panel shows $\Delta GluN1\text{-}AHA$ number of transitions between states over 24 h represented as a percentage over the control $GFP\text{-}AHA$ mice. **D**, Episode number (left) and mean duration (right) allocated by vigilance state and by light and dark period. In **C** data are mean $\pm$ SEM.

$F_{(89,1080)} = 125$, $p < 0.0001$; virus type, $F_{(1,1080)} = 4.3 \times 10^{-10}$, $p = 1$; Fig. 6B). Compared with $GFP\text{-}LPO$ mice, $\Delta GluN1\text{-}LPO$ mice had many more sleep attempts during the SD procedure (Mann–Whitney test, $U = 1$, $p = 0.0006$; Fig. 6C, left panel), and at the end of the 6-h procedure they had a shorter latency to fall asleep (unpaired two-tailed Student's t test, $t = 2.171$, $df = 13$, $p < 0.05$; Fig. 6C, right panel).

During the subsequent first hour of sleep following SD, both $\Delta GluN1\text{-}LPO$ and $GFP\text{-}LPO$ mice had a significant increase in NREM sleep δ power compared with their own baseline at the same circadian time (two-way ANOVA and Sidak's post hoc test: $\Delta GluN1\text{-}LPO$, power, $F_{(89,1080)} = 653$, $p < 0.0001$; virus, $F_{(1,1080)} = 8.9 \times 10^{-9}$, $p = 1$; $GFP\text{-}LPO$, power, $F_{(89,1080)} = 963$, $p < 0.0001$; virus, $F_{(1,1080)} = 7.9 \times 10^{-9}$, $p = 1$; Fig. 6D,E, left panels), showing that, by this measure, sleep homeostasis was intact. The typical diurnal variation in EEG δ power over 24 h seen in control mice was also still present in $\Delta GluN1\text{-}LPO$

←

both $\Delta GluN1\text{-}LPO$ (left) and $GFP\text{-}LPO$ (right) mice. From the top, hypnogram, δ power, EMG, and EEG represented as a somnogram and as a raw trace. **H**, EMG intensity during REM sleep episodes over 25-s time. Values were exported at a 1-Hz sampling rate from raw EMG traces. **I**, Left panel, Episode number for 24-h BL recordings assigned to LP and DP and behavioral state. Center panel, episode mean duration for each behavioral state during LP and DP. Right panel, $\Delta GluN1\text{-}LPO$ mice vigilance state transitions during light (top) and dark (bottom) period represented as percentage over $GFP\text{-}LPO$ transitions. In **C–F**, **I**, data are mean $\pm$ SEM (*$p < 0.05$, **$p < 0.005$, ***$p < 0.0005$, †$p < 0.00005$).
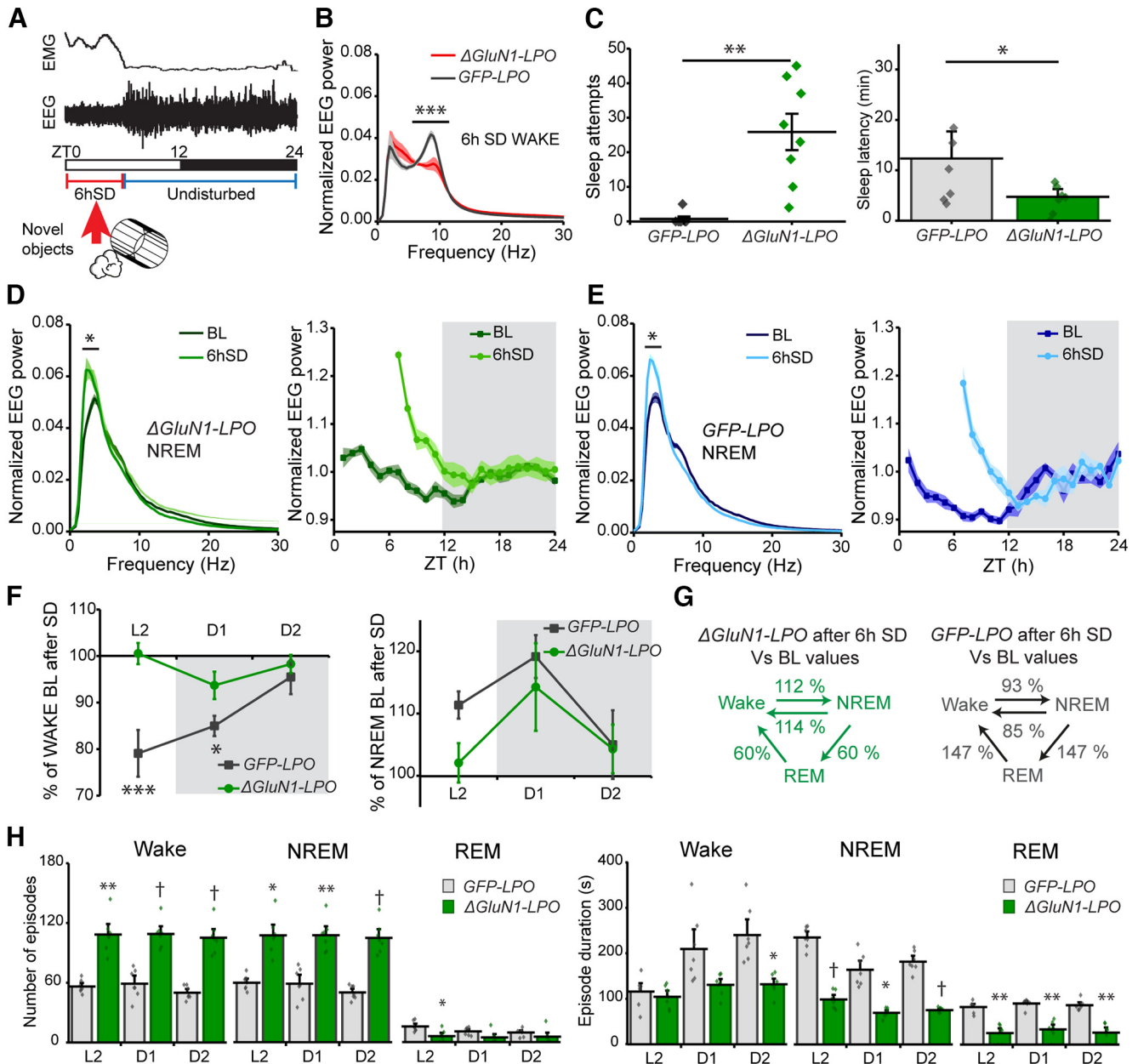
Figure 6. Deletion of the NMDA receptor from LPO does not affect sleep homeostasis and sleep-wake fragmentation persists in the recovery sleep following SD. **A**, Representation of 6-h SD protocol starting when lights turn ON (ZT0), using novel objects to keep the animals awake. For the remaining 18 h, animals are left undisturbed. **B**, Wake EEG power spectrum during 6-h SD. **C**, Number of sleep attempts during the 6-h SD (left) and latency to fall asleep (right) after SD, considering the first NREM sleep bout as at least 30 s long. **D**, **E**, Left panels, NREM sleep EEG power spectrum during 1 h following 6-h SD compared with same circadian time during baseline recordings in $\Delta GluN1$-LPO (**D**) and in GFP-LPO (**E**) mice. Right panels, NREM sleep EEG δ power calculated for every hour during baseline recordings and after 6-h SD in $\Delta GluN1$-LPO and GFP-LPO animals. The EEG power was normalized over the total power during each hour. **F**, Percentage of Wake (left) and NREM sleep (right) amounts in $\Delta GluN1$-LPO and GFP-LPO mice over their own baseline after 6-h SD ZT6–ZT12 (L2), ZT12–ZT18 (D1), ZT18–ZT24 (D2). **G**, Sum of state transitions in the 18 h following 6-h SD presented as a percentage over baseline for both $\Delta GluN1$-LPO and GFP-LPO mice during the same circadian time. **H**, Left panel, Episode number calculated over every 6 h following SD for Wake (left), NREM (center), and REM sleep (right). Right panels, Episode mean duration calculated by 6 h following SD for Wake (left), NREM (center), and REM sleep (right). GFP-LPO, $n = 7$; $\Delta GluN1$-LPO, $n = 7$. Data in all panels **B–F**, **H** are represented as mean ± SEM (*$p < 0.05$, **$p < 0.005$, ***$p < 0.0005$, †$p < 0.00005$).

mice (Fig. 6D,E, right panels). However, $\Delta GluN1$-LPO mice were incapable of recuperating the sleep lost during SD (Fig. 6F, left panel). Following SD as a percentage over their own baselines, GFP-LPO mice as expected increased their time asleep, reducing time spent awake. $\Delta GluN1$-LPO mice, however, did not (two-way ANOVA and Sidak's post hoc test: Wake time, $F_{(1.6,19)} = 5.8$, $p = 0.02$; virus, $F_{(1,12)} = 10.7$, $p = 0.007$; NREM sleep time, $F_{(1.5,17.7)} = 3.2$, $p = 0.08$; virus, $F_{(1,12)} = 2.9$, $p = 0.1$; Fig. 6F, right panel).

After SD, $\Delta GluN1$-LPO animals maintained the highly fragmented sleep phenotype during their recovery sleep, as shown by the percentage of transitions over their own baseline levels. Transitions to and from NREM sleep and Wake were still increased during recovery sleep, and transitions toward REM sleep decreased (paired two-tailed Student's t test, Wake → NREM, 6hSD = 333 ± 16, BL = 303 ± 18, $t = 1.324$, df = 6, $p = 0.23$; NREM → Wake, 6hSD = 317 ± 18, BL = 285 ± 19, $t = 1.296$, df = 6, $p = 0.24$; NREM → REM and REM → Wake,

6hSD = 16 ± 6, BL = 18 ± 5, t = 0.234, df = 6, p = 0.8; Fig. 6G, left panel). On the other hand, *GFP-LPO* control mice had decreased transitions between Wake and NREM sleep when compared with their baseline levels, and had increased transitions toward REM sleep, a sign of efficient recovery sleep (paired two-tailed Student's t test, Wake → NREM, 6hSD = 159 ± 8, BL = 175 ± 10, t = 1.202, df = 6, p = 0.27; NREM → Wake, 6hSD = 124 ± 8, BL = 150 ± 12, t = 2.373, df = 6, p = 0.06; NREM → REM and REM → Wake, 6hSD = 35 ± 4, BL = 25 ± 3, t = 2.785, df = 6, p = 0.03; Fig. 6G, right panel). Additionally, in *ΔGluN1-LPO* mice, NREM sleep and wake episode numbers were still increased, and mean duration decreased after SD (two-way repeated measures ANOVA and Sidak's *post hoc* test: Wake, virus, $F_{(1,12)}$ = 80, p < 0.0001; time, $F_{(1.8,22)}$ = 1.8, p = 0.2; NREM, virus, $F_{(1,12)}$ = 64.8, p < 0.0001; time, $F_{(1.9,23.2)}$ = 1.8, p = 0.2; REM virus, $F_{(1,12)}$ = 6.25, p = 0.03; time, $F_{(1.9,23)}$ = 6.7, p = 0.006; Fig. 6H, left panel), whereas REM sleep values were consistently lower than in *GFP-LPO* mice (two-way repeated measures ANOVA and Sidak's *post hoc* test: Wake, virus, $F_{(1,12)}$ = 17.3, p = 0.001; time, $F_{(1.9,22.6)}$ = 13, p = 0.0002; NREM, virus, $F_{(1,12)}$ = 202.5, p < 0.0001; time, $F_{(1.7,20)}$ = 27, p < 0.0001; REM, virus, $F_{(1,12)}$ = 64, p < 0.0001; time, $F_{(1.8,22)}$ = 2.7, p = 0.1; *GFP-LPO*, n = 7; *ΔGluN1-LPO*, n = 7; Fig. 6H, right panel). The persistence of fragmentation after SD in *ΔGluN1-LPO* mice is noteworthy, as under increased sleep pressure, quantified by the δ power rebound, sleep is deeper compared with baseline levels. These data suggest that *ΔGluN1-LPO* mice were sleepy but could not stay asleep.

Sedatives and sleeping medication transiently improve sleep of mice with NMDA receptors deleted from the LPO hypothalamus

We investigated whether drugs that induce NREM-like sleep, Dex, which is used in intensive care units for long-term sedation (Adams et al., 2013), and zolpidem (Ambien), a widely pre-scribed sleeping medication (Wisden et al., 2019), could reduce the high sleep fragmentation in *ΔGluN1-LPO* mice and restore consolidated sleep. Following intraperitoneal injection, Dex (25 and 50 µg/kg) increased the time spent asleep (two-way repeated measures ANOVA and Tukey's *post hoc* test: for Wake time, time × dose, $F_{(28,210)}$ = 2.4, p = 0.0002; $F_{(6.8,102.5)}$ = 3.2, p = 0.004; dose, $F_{(2,15)}$ = 8.1, p = 0.004; for NREM sleep time × dose, $F_{(28,210)}$ = 2.8, p < 0.0001; time, $F_{(6.8,101.5)}$ = 3.7, p = 0.002; dose, $F_{(2,15)}$ = 7.6, p = 0.005; For REM sleep time × dose, $F_{(28,210)}$ = 2.4, p = 0.0002; time, $F_{(5.4,80.9)}$ = 13.7, p < 0.0001; dose, $F_{(2,15)}$ = 1.8, p = 0.2, n = 6; Fig. 7A) and transiently changed, depending on the dose, the number of NREM sleep episodes (two-way repeated measures ANOVA and Tukey's *post hoc* test: time × dose, $F_{(28,210)}$ = 2.87, p < 0.0001; time, $F_{(6.2,92.5)}$ = 1.85, p = 0.1; dose, $F_{(2,15)}$ = 1.7, p = 0.3; Fig. 7B, left panel) and increased NREM sleep episode mean duration for 1 h after injection in *ΔGluN1-LPO* mice (two-way repeated measures ANOVA and Tukey's *post hoc* test: time × dose, $F_{(28,210)}$ = 5.5, p < 0.0001; time, $F_{(1.3,19)}$ = 5.7, p = 0.02; dose, $F_{(2,15)}$ = 6.5, p = 0.009; Fig. 7B, right panel). Similarly, zolpidem (5 mg/kg) increased sleep time, and decreased wakefulness during the 6 h postinjection period (two-way repeated measures ANOVA and Tukey's *post hoc* test: for Wake time × drug, $F_{(12,96)}$ = 3.61, p = 0.0002; time, $F_{(4.3,34.7)}$ = 1.6, p = 0.2; dose, $F_{(1,8)}$ = 6.4, p = 0.04; for NREM sleep time × drug, $F_{(12,96)}$ = 3.98, p < 0.0001; time, $F_{(4.4,35)}$ = 1.6 p = 0.2; dose, $F_{(1,8)}$ = 6, p = 0.04; for REM sleep time × drug, $F_{(12,96)}$ = 2.3, p = 0.01; time, $F_{(4.3,34.5)}$ = 4.4, p = 0.005; dose, $F_{(1,8)}$ = 2.2, p = 0.2, n = 6; Fig. 7C). However, zolpidem did not affect the number of

NREM sleep episodes (two-way repeated measures ANOVA and Tukey's *post hoc* test: time × dose, $F_{(12,96)}$ = 1.8, p = 0.6; time, $F_{(5.5,44)}$ = 2, p = 0.07; dose, $F_{(1,8)}$ = 0.7, p = 0.4, n = 6; Fig. 7D, left panel), but it increased their duration (two-way repeated measures ANOVA and Tukey's *post hoc* test: time × dose, $F_{(12,96)}$ = 2.5, p = 0.007; time, $F_{(12,96)}$ = 0.8, p = 0.7; dose, $F_{(1,8)}$ = 3, p = 0.1; Fig. 7D, right panel). For both Dex and zolpidem, a few hours af-ter drug administration the highly fragmented sleep pattern re-emerged (data not shown).

Both doses of Dex (25 and 50 µg/kg), and zolpidem (5 mg/kg), had a similar effect on control *GFP-LPO* mice, increasing their NREM sleep time, while decreasing Wake and REM sleep times (two-way repeated measures ANOVA and Dunnett's *post hoc* test: for Wake time × drug, $F_{(15,100)}$ = 12.44, p < 0.0001; time, $F_{(3.2,63.8)}$ = 2.7, p = 0.5; dose, $F_{(3,20)}$ = 19.7, p < 0.0001; for NREM sleep time × drug, $F_{(15,100)}$ = 11.4, p < 0.0001; time, $F_{(3.2,65.2)}$ = 6.4, p = 0.0005; dose, $F_{(3,20)}$ = 28.9, p < 0.0001; for REM sleep time × drug, $F_{(15,100)}$ = 3.8, p < 0.0001; time, $F_{(2.5,49.6)}$ = 17.1, p < 0.0001; dose, $F_{(3,20)}$ = 38, p < 0.0001, n = 6; Fig. 7E). Dex (50 µg/kg) and zolpidem, also decreased the number of NREM sleep episodes (two-way repeated measures ANOVA and Dunnett's *post hoc* test: time × drug, $F_{(15,100)}$ = 2.3, p = 0.007; time, $F_{(2.9,59)}$ = 2.8, p = 0.048; drug, $F_{(3,20)}$ = 4.4, p = 0.015; Fig. 7F, left panel) and increased NREM sleep average duration (two-way repeated measures ANOVA and Dunnett's *post hoc* test: time × drug, $F_{(15,100)}$ = 1.02, p = 0.44; time, $F_{(1.5,30.8)}$ = 1.2, p = 0.3; drug, $F_{(3,20)}$ = 10.6, p = 0.0002; Fig. 7F, right panel).

Sleep fragmentation but not sleep loss is produced by selective NMDA GluN1 subunit knock-down in GABA LPO neurons but not glutamate LPO neurons

To investigate the NR1-expressing LPO cell types involved in regulating sleep, we could not use Cre recombinase to ablate the *Grin1* gene because no cell type-selective promoters are avail-able to restrict NR1 deletion selectively to subtypes of LPO cells without also affecting other brain areas. We therefore decided to use shRNA transgenes to reduce GluN1 expression cell-type selectively, for example, in GABAergic or glutamatergic cells in LPO (see Materials and Methods). First, we tested the ef-ficacy of three different shRNAs to knock-down recombinant GluN1-mCherry cDNA expression (Fig. 8A,B). Having identified a suitable shRNA, shRNA3, that significantly reduced GluN1-mCherry cDNA expression compared with scrambled shRNA (one-way ANOVA: $F_{(3,44)}$ = 9.13, p < 0.0001; Tukey's *post hoc* test: Scramble vs shRNA3 p = 0.0007, shRNA1 vs shRNA3 p = 0.0003, shRNA2 vs shRNA3 p = 0.0008, n = 10 transfec-tions; Fig. 8B), the shRNA was cloned into an AAV transgene cassette (see Materials and Methods), and *AAV-flex-shRNA-GluN1* and *AAV-flex-shRNA-scramble* (*scr*) viruses were then bilaterally injected into the LPO areas of *Vglut2-Cre* and *Vgat-Cre* mice to generate *Vglut2-shRNA-GluN1-LPO* and *Vgat-shRNA-GluN1-LPO* mice and the associated scramble control, respectively (Figs. 8C, 9A).

For the *Vglut2-shRNA-GluN1-LPO* mice, and unlike the *ΔGluN1-LPO* mice, the macrostructure of vigilance states was unchanged: *Vglut2-shRNA-GluN1-LPO* mice did not have sleep loss compared with scramble shRNA controls (two-way ANOVA and Sidak's *post hoc* test: for the light phase, vigilance state, $F_{(2,33)}$ = 760, p < 0.0001; virus, $F_{(1,33)}$ = 2.8 × 10^{-6}, p = 1; for the dark phase, vigilance state, $F_{(2,33)}$ = 374, p < 0.0001; vi-rus, $F_{(1,33)}$ = 1.3 × 10^{-7}, p = 1; Fig. 8D). The EEG power
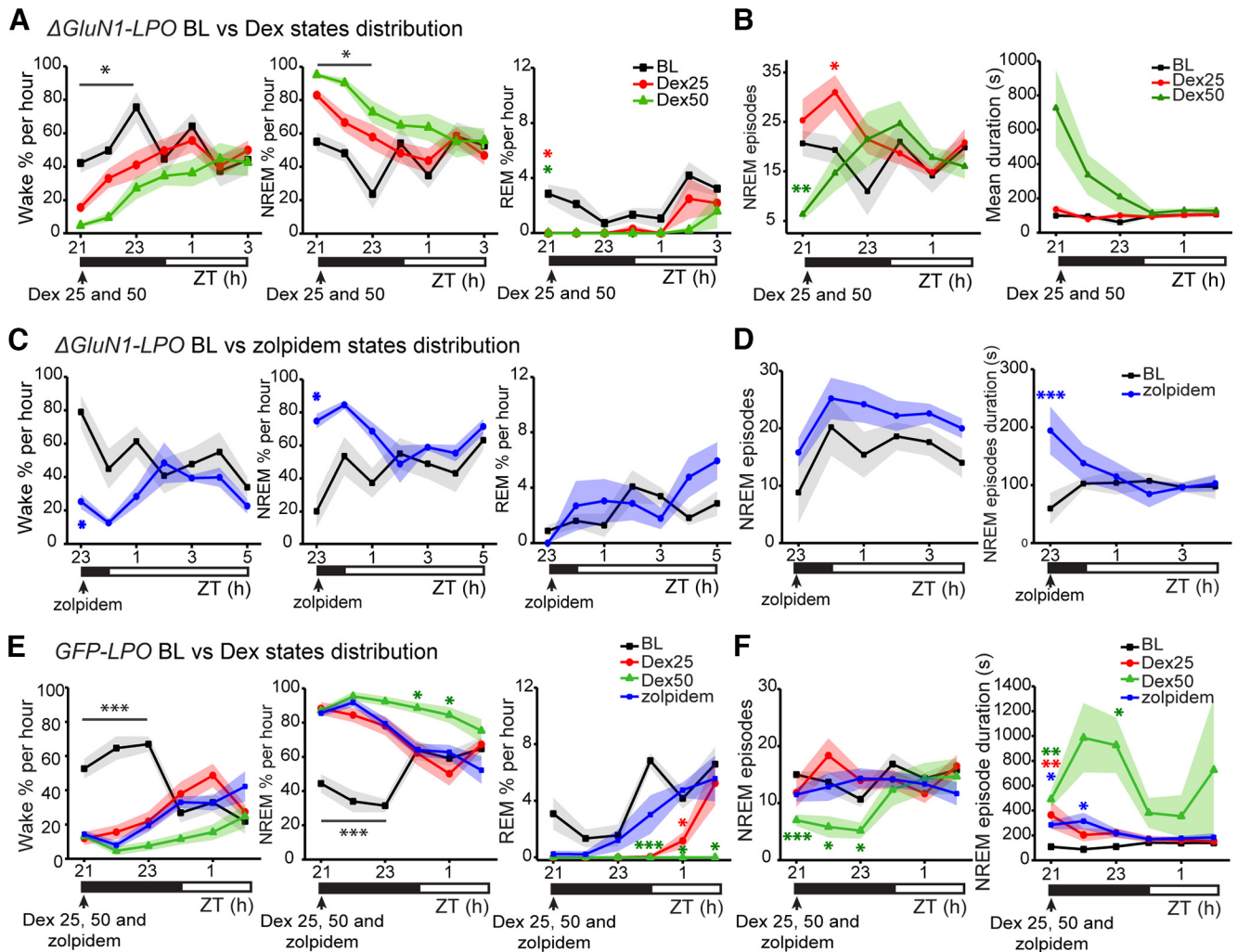
Figure 7. Dex and zolpidem both increased sleep time and Dex reduced sleep fragmentation in mice lacking NMDA receptors in LPO. **A**, ΔGluN1-LPO baseline (BL) states distribution as percentage of 1 h in Wake (left), NREM (center), and REM sleep (right) compared with the distribution after intraperitoneal injection of Dex 25 μg/kg (red) and 50 μg/kg (green) at ZT21. **B**, ΔGluN1-LPO number of NREM sleep episodes (left) and NREM sleep episode mean duration (right) comparing BL to Dex sleep recordings. **C**, ΔGluN1-LPO distribution by hour of Wake (left), NREM (center), and REM sleep (right) following intraperitoneal injection of zolpidem (5 mg/kg) at ZT23. **D**, NREM sleep episode number (left) and mean duration (right) comparing BL to zolpidem sleep recordings in ΔGluN1-LPO mice. **E**, GFP-LPO BL state distribution as percentage of 1 h in Wake (left), NREM (center), and REM sleep (right) compared with the distribution after injection at ZT21 of Dex 25 μg/kg (red), Dex 50 μg/kg (green), and zolpidem 5 mg/kg (blue). **F**, Control GFP-LPO number of NREM sleep episodes (left) and NREM sleep episode mean duration (right) comparing BL to Dex and to zolpidem. For panels **A–D**, ΔGluN1-LPO, n = 6. For panels **E**, **F**, GFP-LPO, n = 6. Data in all panels are represented as mean ± SEM (*p < 0.05, **p < 0.005, ***p < 0.005). Asterixis in black indicate significant difference from baseline values for each drug and dose tested. Asterixis in red, green, and blue indicated significant differences from BL values only for Dex 25 μg/kg, Dex 50 μg/kg, and zolpidem, respectively.

spectra during Wake, NREM, and REM sleep were also typical (Fig. 8E).

Vglut2-shRNA-GluN1-LPO mice did not have a sleep-wake fragmentation phenotype, the number of vigilance state episodes was unchanged compared with scramble shRNA controls (two-way ANOVA and Sidak's *post hoc* test: vigilance state, $F_{(5,66)} = 58$, $p < 0.0001$; virus, $F_{(1,66)} = 2.8$, $p = 0.1$; Fig. 8F, left panel), the mean duration of vigilance states was the same as in mice injected with scramble shRNA controls (two-way ANOVA and Sidak's *post hoc* test: vigilance state, $F_{(5,66)} = 17.6$, $p < 0.0001$; virus, $F_{(1,66)} = 1$, $p = 0.3$; Fig. 8F, center panel), as was the number of transitions between states represented as percentage over number of transitions in Vglut2-shRNA-scr-LPO mice was also similar (unpaired two-tailed Student's *t* test, Wake → NREM, Vglut2-shRNA-GluN1-LPO = 356.5 ± 37, Vglut2-shRNA-scr-LPO = 405 ± 31 transitions, $t = 1.009$, df = 11, $p = 0.3$; NREM → Wake, Vglut2-shRNA-GluN1-LPO = 276 ± 34, Vglut2-shRNA-scr-LPO = 333 ± 31 transitions, $t = 1.252$, df = 11, $p = 0.2$; NREM →

REM and REM → Wake, Vglut2-shRNA-GluN1-LPO = 81 ± 4, Vglut2-shRNA-scr-LPO = 73 ± 3 transitions, $t = 1.629$, df = 11, $p = 0.1$; Fig. 8F, right panel).

For the Vgat-shRNA-GluN1-LPO mice (Fig. 9A), we confirmed that the AAV-flex-shRNA-GluN1 transgene expression was confined largely to LPO (Fig. 9B,C). We tested the efficiency of NMDA receptor knock-down by recording evoked EPSCs on Vgat-LPO neurons in acute hypothalamic slices. Vgat-shRNA-GluN1-LPO cells visibly showed a reduction in NMDA receptor-mediated currents compared with Vgat-shRNA-scr-LPO control cells and the NMDA/AMPA ratio was significantly reduced in Vgat-shRNA-GluN1-LPO cells (Fig. 9D), demonstrating that Vgat-LPO neurons in Vgat-shRNA-GluN1-LPO mice have similar degree of NMDA receptor-mediated current deficiency as ΔGluN1-LPO neurons with the Cre-mediated disruption of the grin1 gene (two-tailed Mann–Whitney test, $U = 0$, $p = 0.008$. Vgat-shRNA-scr-LPO, n = 5; Vgat-shRNA-GluN1-LPO, n = 5; Fig. 9D, right panel).
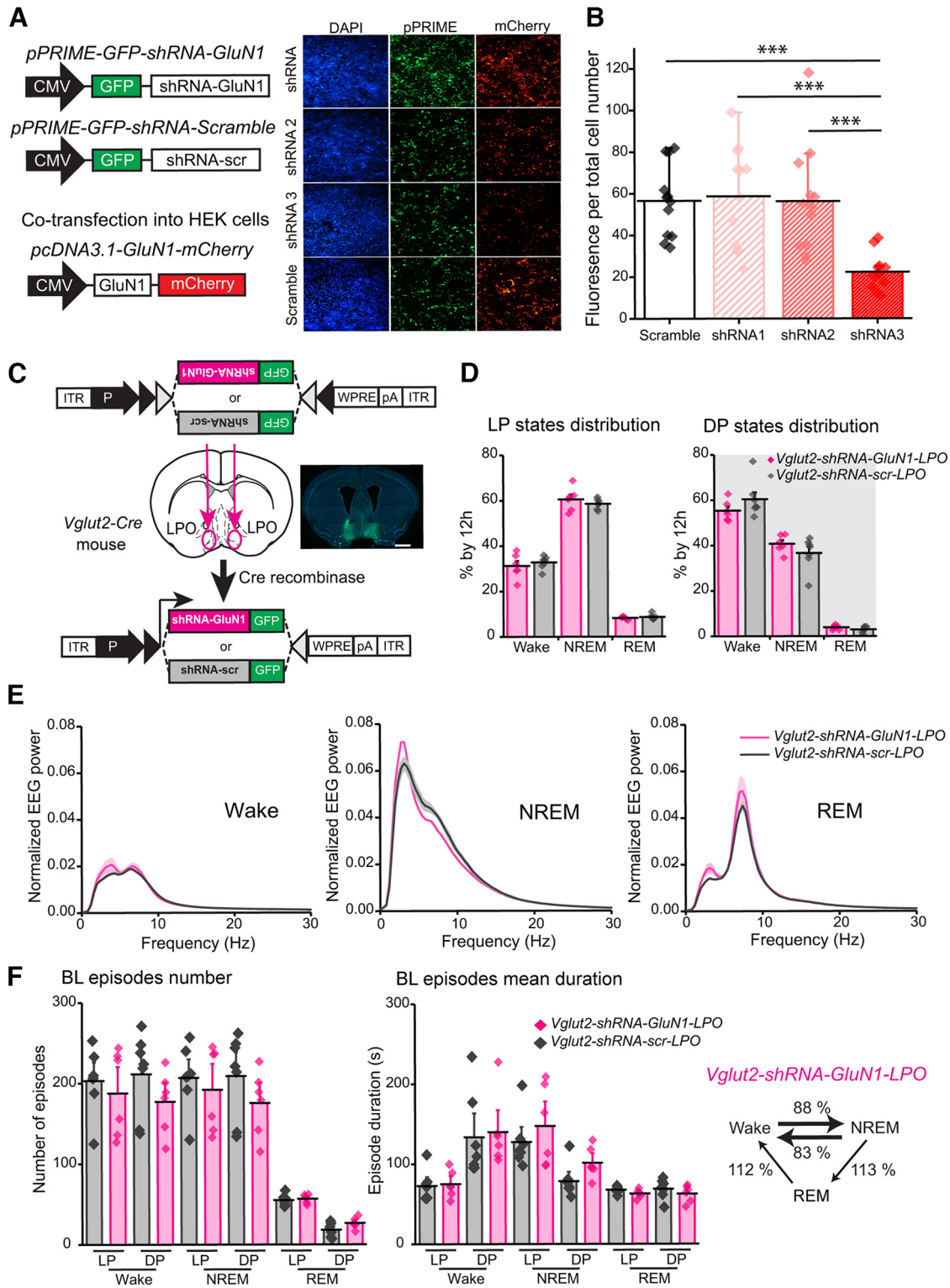
Figure 8. Knock-down of the NMDA receptor GluN1 subunit from *Vglut2*-expressing LPO neurons does not alter sleep and Wake patterns. *A*, Plasmid DNA constructs used to test *shRNA-GluN1* efficiency (left) and fluorescent images (right) of transfected HEK293 cells showing DAPI (left column, in blue), GFP reporter for expression of *shRNA-GluN1* and shRNA-scramble *pPRIME* vectors (central column, in green), and mCherry reporter expression, which indicates expression of the plasmid carrying the GluN1 sequence (right column, in red). *B*, Quantification of mCherry fluorescence per total cell number after transfection of HEK293 cells with plasmids expressing the shRNA-GluN1 or the control scramble shRNA. *C*, *shRNA-GluN1* or *shRNA-scr* AAVs were bilaterally injected into the LPO of *Vglut2-Cre* mice. Right, Immunohistochemistry to map viral vector expression (GFP in green, DAPI in blue). Scale bar: 1 mm. *D*, Baseline (BL) vigilance state amounts calculated as a percentage over 12 h of the light (LP, left) and dark (DP, right) periods. *E*, EEG power spectrum for Wake (left), NREM (center), and REM sleep (right) during 12-h light period normalized over the total EEG power. *F*, Left panel, BL episode number over 12 h comparing *Vglut2-shRNA-GluN1-LPO* and *Vglut2-shRNA-scr-LPO* mice. Center panel, Episodes mean duration by 12 h during BL recordings. Right panel, *Vglut2-shRNA-GluN1-LPO* number of transitions between states represented as percentage over the *Vglut2-shRNA-scr-LPO* BL. *Vglut2-shRNA-GluN1-LPO*, *n* = 6; *Vglut2-shRNA-scr-LPO*, *n* = 7. In *B–D*, data are represented as mean ± SEM.
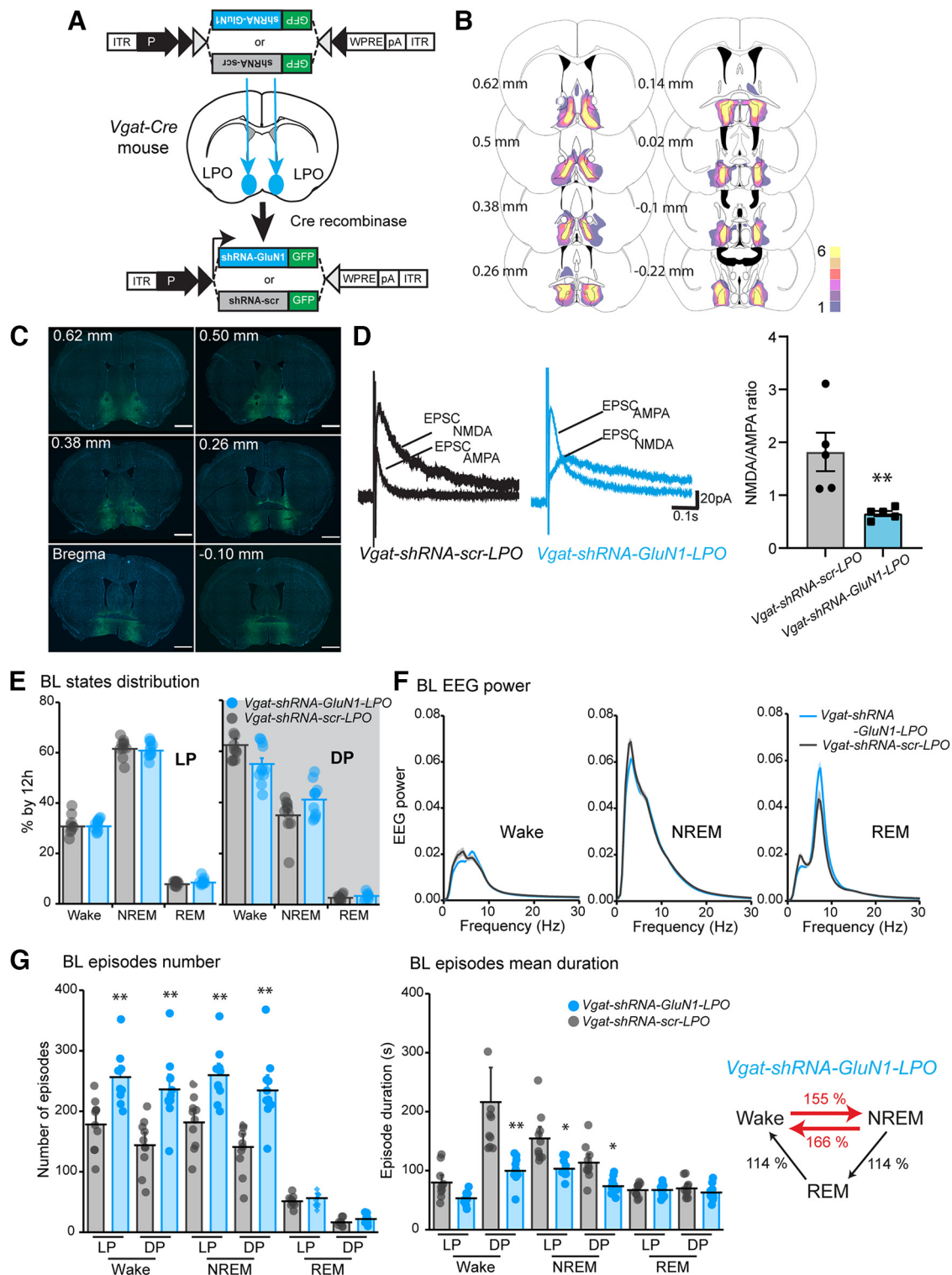
Figure 9. NMDA receptor GluN1 knock-down from GABA neurons in the LPO causes sleep-wake fragmentation but not sleep loss. ***A***, *AAV-flex-shRNA-GluN1* or *AAV-flex-shRNA-scramble* (scr) were bilaterally injected in the LPO area of *Vgat-cre* mice to generate *Vgat-shRNA-GluN1-LPO* and *Vgat-shRNA-scr-LPO* mice. ***B***, Schematic representation of *AAV-flex-shRNA-GluN1* expression in the LPO of *Vgat-Cre* mice used for sleep recordings. In the heat map, yellow corresponds to areas were all six mice showed GFP-positive cells, whereas dark purple indicates areas where only 1 mouse showed GFP-positive cells. Coordinates are relative to bregma. ***C***, Mapping of shRNA transgene expression using immunohistochemistry (*shRNA-GluN1* expressing GFP in green; DAPI in blue). Coordinates are relative to bregma. Scale bars: 1 mm. ***D***, Left panel, Example traces of NMDA receptor-mediated and AMPA receptor-mediated currents (labeled as EPSC$_{NMDA}$ and EPSC$_{AMPA}$, respectively) in *Vgat-shRNA-scr-LPO* (in black) and *vgat-shRNA-GluN1-LPO* (in blue) cells. Right panel, NMDA/AMPA ratio in *Vgat-shRNA-scr-LPO* and *Vgat-shRNA-GluN1-LPO* neurons, showing a decrease in NMDA current in neurons expressing *shRNA-GluN1* compared with controls. ***E***, Vigilance state distribution represented as a percentage of 12 h during light (LP, left) and dark (DP, right) periods for *Vgat shRNA-GluN1-LPO* and *Vgat-shRNA-scr-LPO* mice. ***F***, EEG power spectrum of Wake (left), NREM (center), and REM (right) sleep during 12-h light period in *Vgat-shRNA-GluN1* mice normalized over total EEG power. ***G***, Left and center panels, Baseline episode number (left) and episode mean duration (center) comparing *Vgat-shRNA-GluN1-LPO* with control *Vgat shRNA-scr-LPO* mice. Right panel, Number of transitions in *Vgat-shRNA-GluN1-LPO* mice represented as percentage over control group during 24-h baseline recordings. *Vgat-shRNA-GluN1-LPO, n = 12; Vgat-shRNA-scr-LPO, n = 11*. In ***B***, ***D–F***, data are represented as mean ± SEM. In ***F***, *p < 0.05, **p < 0.005.

We next looked at the sleep phenotype of *Vgat-shRNA-GluN1-LPO* mice. The overall macrostructure of vigilance states was not changed: *Vgat-shRNA-GluN1-LPO* mice did not have sleep loss compared with the respective scramble shRNA controls (two-way ANOVA and Sidak's *post hoc* test: vigilance state, $F_{(5,113)} = 564$, $p < 0.0001$; virus, $F_{(1,113)} = 0.03$, $p = 0.9$; Fig. 9E). The EEG power spectra during Wake, NREM, and REM sleep were also not different (Fig. 9F). However, for *Vgat-shRNA-GluN1-LPO* mice, there were more Wake and NREM sleep episodes (two-way ANOVA and Sidak's *post hoc* test: episode number, $F_{(5,114)} = 110$, $p < 0.0001$; virus, $F_{(1,114)} = 73$, $p < 0.0001$; Fig. 9G, left panel), and decreased in episode duration resembling the sleep fragmentation phenotype observed in $\Delta GluN1$-LPO mice (two-way ANOVA and Sidak's *post hoc* test: mean duration, $F_{(5,114)} = 39$, $p < 0.0001$; virus, $F_{(1,114)} = 62$, $p < 0.0001$; Fig. 9G, center panel). Additionally, there was a >55% increase in transitions between vigilance states in *Vgat-shRNA-GluN1-LPO* mice compared with *Vgat-shRNA-scr-LPO* mice (unpaired two-tailed Student's *t* test, Wake → NREM, *Vgat-shRNA-GluN1-LPO* = 484 ± 28, *Vgat-shRNA-scr-LPO* = 312 ± 25 transitions, $t = 4.594$, df = 19, $p = 0.0002$; NREM → Wake, *Vgat-shRNA-GluN1-LPO* = 408 ± 30, *Vgat-shRNA-scr-LPO* = 246 ± 26 transitions, $t = 4.09$, df = 19, $p = 0.0006$; NREM → REM and REM → Wake, *Vgat-shRNA-GluN1-LPO* = 76 ± 6 transitions, *Vgat-shRNA-scr-LPO* = 66 ± 3 transitions, $t = 1.409$, df = 19, $p = 0.2$; Fig. 9G, right panel).

As for the $\Delta GluN1$-LPO mice with the NMDA receptors removed from all cell types in the LPO area, we next tested whether the sleep-wake fragmentation phenotype of *Vgat-shRNA-GluN1-LPO* mice persisted under conditions of raised sleep pressure following 6 h of SD. In contrast to mice with GluN1 deletion from all neuronal cell types in LPO, *Vgat-shRNA-GluN1-LPO* mice did not show a "sleepy phenotype," as their sleep attempts during SD did not differ from the control group (Kolmogorov–Smirnov test, *Vgat-shRNA-GluN1-LPO*, $n = 10$; *Vgat-shRNA-scr-LPO*, $n = 9$, $p = 0.5$; Fig. 10A). Following 6-h SD, *Vgat-shRNA-GluN1-LPO* mice had a significant increase in the EEG δ power during the 1 h following SD compared with their own baseline power, similarly to $\Delta GluN1$-LPO mice, showing that sleep homeostasis was intact (two-way ANOVA and Sidak's *post hoc* test: for *Vgat-shRNA-GluN1-LPO* mice, frequency, $F_{(89,1620)} = 614$, $p < 0.0001$; virus, $F_{(1,1620)} = 1$, $p = 0.3$; for *Vgat-shRNA-scr-LPO* mice, frequency, $F_{(89,1620)} = 624$, $p < 0.0001$; virus, $F_{(1,1620)} = 2$, $p = 0.1$, *Vgat-shRNA-GluN1-LPO*, $n = 10$; mice; *Vgat-shRNA-scr-LPO*, $n = 9$ mice; Fig. 10B). *Vgat-shRNA-GluN1-LPO* mice maintained the fragmented sleep phenotype under high sleep pressure, with more transitions between states (unpaired two-tailed Student's *t* test, Wake → NREM, *Vgat-shRNA-GluN1-LPO* = 368 ± 19.4, *Vgat-shRNA-scr-LPO* = 221 ± 10.5 transitions, $t = 6.43$, df = 17, $p < 0.0005$; NREM → Wake, *Vgat-shRNA-GluN1-LPO* = 297 ± 18, *Vgat-shRNA-scr-LPO* = 156 ± 10, $t = 6.6$, df = 17, $p < 0.0005$; NREM → REM and REM → Wake, *Vgat-shRNA-GluN1-LPO* = 71 ± 4, *Vgat-shRNA-scr-LPO* = 64 ± 4 transitions, $t = 1.097$, df = 17, $p = 0.3$; Fig. 10C), and more wake and NREM episodes (two-way repeated measures ANOVA and Sidak's *post hoc* test: vigilance state, $F_{(2.5,43)} = 218$, $p < 0.0001$; virus, $F_{(1,17)} = 37$, $p < 0.0001$; Fig. 10D), and with decreased mean durations compared with *Vgat-shRNA-scr-LPO* mice (two-way repeated measures ANOVA and Sidak's *post hoc* test: vigilance state, $F_{(4.8,81)} = 56$, $p < 0.0001$; virus, $F_{(1,17)} = 40$, $p < 0.0001$). *Vgat-shRNA-GluN1-LPO*, $n = 10$; *Vgat-shRNA-scr-LPO*, $n = 9$ mice; Fig. 10E). Thus, the sleep-wake fragmentation aspect but not the

REM sleep loss of $\Delta GluN1$-LPO mice originates from GABA cells in LPO.

Sedatives and sleeping medications improve sleep in mice lacking NMDA receptors in LPO GABA neurons

Next, we tested the effects on sleep fragmentation in *Vgat-shRNA-GluN1-LPO* mice by using the sedative drug Dex and the sleep drug zolpidem. Both doses of Dex (25 and 50 µg/kg), and zolpidem (5 mg/kg), injected into *Vgat-shRNA-GluN1-LPO* mice reduced Wake and REM sleep times, increasing the time spent in NREM sleep (two-way repeated measures ANOVA and Dunnett's *post hoc* test: for Wake time × drug, $F_{(15,60)} = 2.7$, $p = 0.003$; time, $F_{(2.7,32)} = 6.1$, $p = 0.0028$; dose, $F_{(3,12)} = 15.2$, $p = 0.0002$; for NREM sleep time × drug, $F_{(15,60)} = 3.1$, $p = 0.001$; time, $F_{(2.6,31.5)} = 7.8$, $p = 0.0008$; dose, $F_{(3,12)} = 22.7$, $p < 0.0001$; for REM sleep time × drug, $F_{(15,60)} = 2.9$, $p = 0.002$; time, $F_{(2.4,28.9)} = 1.7$, $p = 0.2$; dose, $F_{(3,12)} = 20.2$, $p < 0.0001$, $n = 4$ mice; Fig. 11A). Looking at the sleep architecture, Dex (25 and 50 µg/kg) transiently decreased the NREM sleep episode number, while zolpidem increased (two-way repeated measures ANOVA and Dunnett's *post hoc* test: time × drug, $F_{(15,60)} = 2.5$, $p = 0.007$; time, $F_{(3.2,38)} = 1.7$, $p = 0.2$; drug, $F_{(3,20)} = 2.8$, $p = 0.08$; Fig. 11B, left panel). Both doses of Dex increased the NREM average episode duration, while zolpidem had no effects in maintaining longer NREM sleep bouts (two-way repeated measures ANOVA and Dunnett's *post hoc* test: time × drug, $F_{(15,60)} = 3.6$, $p = 0.0002$; time, $F_{(2,24.3)} = 8.3$, $p = 0.002$; drug, $F_{(3,12)} = 6.7$, $p = 0.007$; Fig. 11B, right panel). A similar effect was also present in control *Vgat-shRNA-scr-LPO* mice, where we observed an increase in NREM sleep time and a decrease in time mice spent awake and in REM sleep when mice were injected with Dex and zolpidem (two-way repeated measures ANOVA and Dunnett's *post hoc* test: for wake time × drug, $F_{(15,100)} = 2.7$, $p = 0.002$; time, $F_{(3.6,72)} = 3.5$, $p = 0.01$; dose, $F_{(3,20)} = 78.4$, $p < 0.0001$; for NREM sleep time × drug, $F_{(15,100)} = 3.2$, $p = 0.0003$; time, $F_{(3.7,74.2)} = 4.8$, $p = 0.002$; dose, $F_{(3,20)} = 107.6$, $p < 0.0001$; for REM sleep time × drug, $F_{(15,100)} = 1.9$, $p = 0.03$; time, $F_{(3.2,65)} = 1.9$, $p = 0.13$; dose, $F_{(3,20)} = 34.6$, $p < 0.0001$, $n = 6$ mice; Fig. 11C). As for *Vgat-shRNA-GluN1-LPO* mice, *Vgat-shRNA-scr-LPO* mice did not show changes in NREM sleep architecture after zolpidem injection. NREM sleep episodes only decreased with zolpidem (two-way repeated measures ANOVA and Dunnett's *post hoc* test: time × drug, $F_{(15,100)} = 1.3$, $p = 0.2$; time, $F_{(3.4,67.8)} = 5.6$, $p = 0.001$; drug, $F_{(3,20)} = 11.8$, $p = 0.0001$; Fig. 11D, left panel), while NREM sleep mean duration briefly increased after Dex 25 µg/kg injection, and a more prolonged increase occurred when 50 µg/kg of Dex was injected (two-way repeated measures ANOVA and Dunnett's *post hoc* test: time × drug, $F_{(15,100)} = 5.1$, $p < 0.0001$; time, $F_{(2.5,49.7)} = 8.7$, $p = 0.0002$; drug, $F_{(3,20)} = 20.6$, $p < 0.0001$; Fig. 11D, right panel). Thus, sedatives and sleeping medications can transiently remove the insomnia (sleep-wake fragmentation) in mice lacking NMDA receptors in LPO GABA neurons.

Discussion

The PO hypothalamus is required for both NREM and REM sleep generation and NREM sleep homeostasis (Nauta, 1946; McGinty and Sterman, 1968; Sherin et al., 1996; John and Kumar, 1998; Lu et al., 2000, 2002; Szymusiak et al., 2007; Zhang et al., 2015; Ma et al., 2019; Reichert et al., 2019). We explored how NMDA receptors on LPO neurons regulate sleep. Deleting the core GluN1 subunit of NMDA receptors from LPO neurons
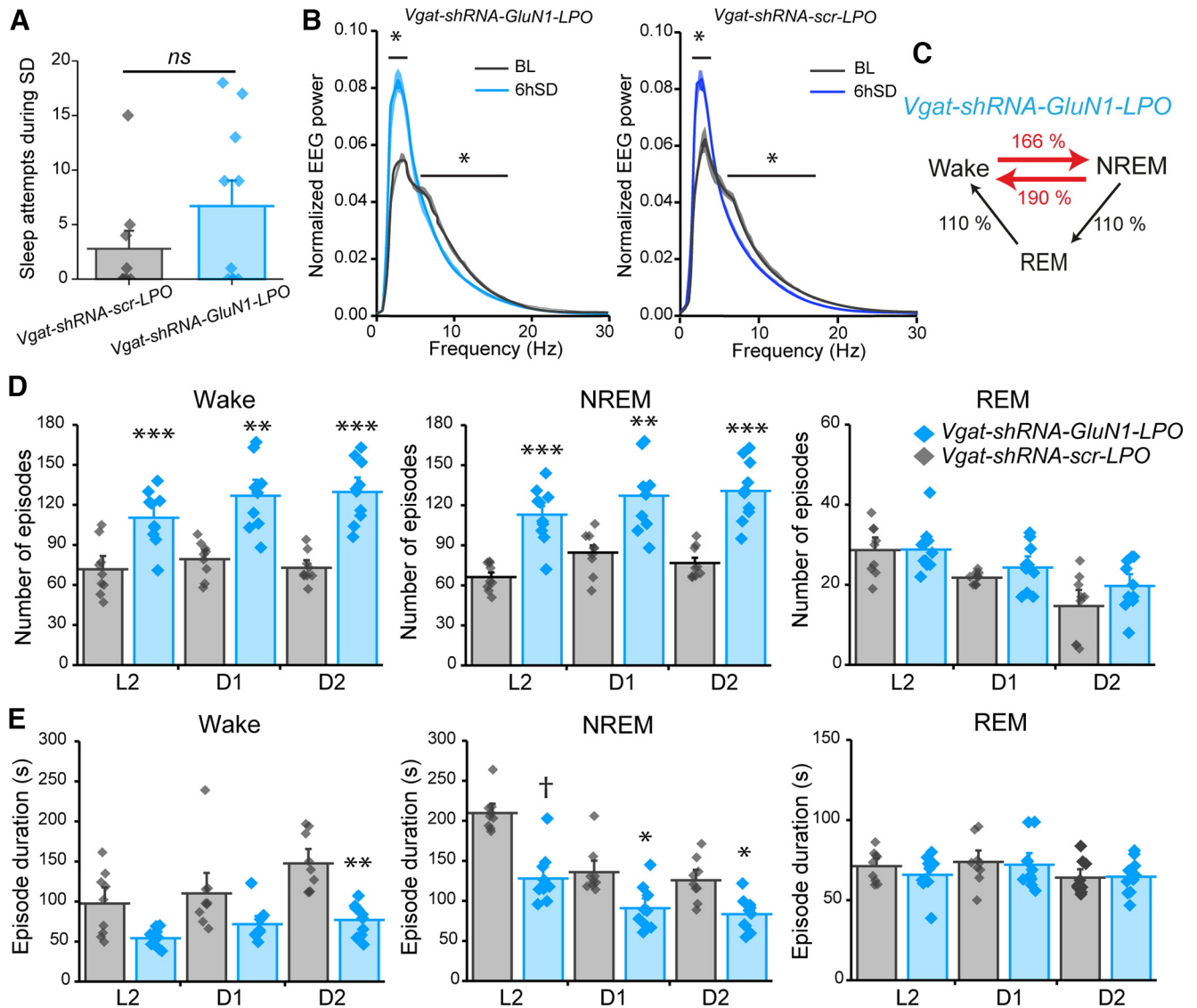
Figure 10. *Vgat-shRNA-GluN1-LPO* mice still have fragmented sleep after 6-h SD. ***A***, Number of NREM sleep attempts during 6-h SD comparing *Vgat-shRNA-GluN1-LPO* with *Vgat-shRNA-scr-LPO* mice. ***B***, NREM EEG power spectrum comparing 1 h after SD to the same circadian time during baseline recordings, to represent EEG δ power rebound in *Vgat-shRNA-GluN1-LPO* (left) and *Vgat-shRNA-scr-LPO* (right) mice. ***C***, Number of transitions for *Vgat-shRNA-GluN1-LPO* mice during the 18 h following 6-h SD represented as a percentage over the number of transitions exhibited by *Vgat-shRNA-scr-LPO* control mice. ***D***, Episode number during Wake (left), NREM (center), and REM sleep (right) following 6-h SD ZT6–ZT12 (L2), ZT12–ZT18 (D1), ZT18–ZT24 (D2). ***E***, Episode mean duration following 6-h SD for Wake (left), NREM (center), and REM sleep (right). *Vgat-shRNA-GluN1-LPO*, $n = 10$; *Vgat-shRNA-scr-LPO*, $n = 9$. Data in ***A***, ***B***, ***D***, ***E*** are mean ± SEM. In ***B***, ***D***, ***E***, $p < 0.05$, **$p < 0.005$, ***$p < 0.0005$, †$p < 0.00005$.

substantially reduced the excitatory drive onto these cells and abolished activity during all vigilance states. These $\Delta GluN1$-LPO mice had less NREM sleep and altered REM sleep patterns (atonia was present, but there was reduced EEG θ activation). In addition, $\Delta GluN1$-LPO mice had highly fragmented sleep-wake: they had many more episodes of wake and NREM sleep, but each episode was shorter. Thus, although $\Delta GluN1$-LPO mice can still enter NREM sleep from wake, AMPA glutamate receptor excitation alone on LPO sleep-promoting neurons is insufficient to maintain NREM sleep or produce REM sleep. The $\Delta GluN1$-LPO mice phenotype is quite similar (Wake-NREM fragmentation, loss of REM sleep) to mice with a double (global) deletion of the muscarinic receptor genes *Chrm1* and *Chrm3* (Niwa et al., 2018), so this could intersect on the same pathway. The phenotype was further stratified. High sleep-wake fragmentation, but not sleep loss, was produced by selective GluN1 knock-down in GABAergic LPO neurons (*Vgat-shRNA-GluN1-LPO* mice).

The molecular mechanism of sleep homeostasis, whereby the time spent awake is tracked and leads to an increase drive to sleep, is not resolved. A mutation in one kinase, salt-inducible kinase3, which is expressed throughout the brain, reduces sleep homeostasis (Funato et al., 2016; Honda et al., 2018). In regions such as neocortex and hippocampus, increased time awake leads to increased phosphorylation of hundreds of synaptic proteins, including glutamate receptors (Wang et al., 2018; Brüning et al., 2019). Calcium entry through NMDA receptors has been suggested to be part of the sleep homeostasis mechanism that tracks time spent awake, and the calcium entry through NMDA receptors could stimulate phosphorylation (Liu et al., 2016; Tatsuki et al., 2016). But at least for the PO hypothalamus, which contains galanin neurons required for sleep homeostasis (Ma et al., 2019; Reichert et al., 2019), our findings show that NMDA receptors are not needed for sleep homeostasis.
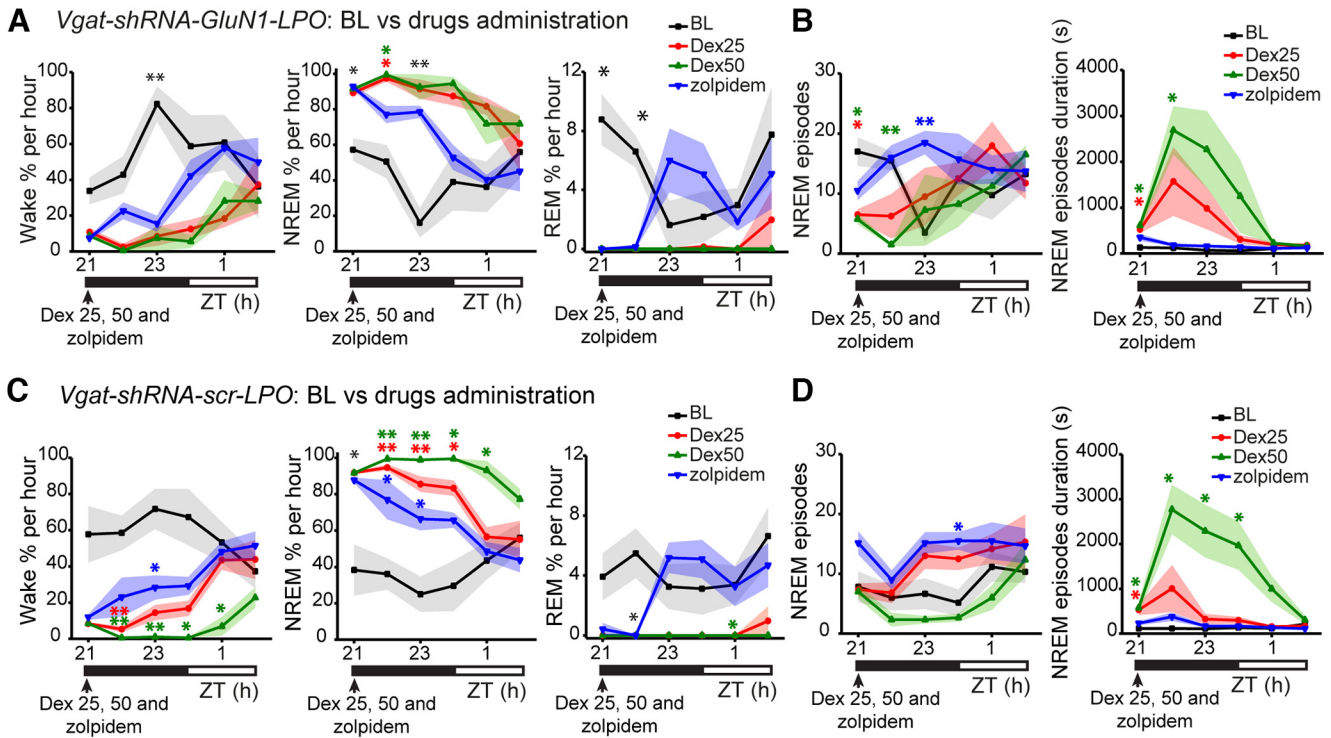
Figure 11. A sedative (Dex) and sleeping medication (zolpidem) reduce sleep fragmentation in *Vgat-shRNA-GluN1-LPO* mice. *A*, *Vgat-shRNA-GluN1* mice BL vigilance state distribution as percentage of 1 h in Wake (left), NREM (center), and REM sleep (right) compared with the distribution after injection at ZT21 of Dex 25 μg/kg (red), Dex 50 μg/kg (green), and zolpidem 5 mg/kg (blue). *B*, *Vgat-shRNA-GluN1-LPO* number of NREM episodes (left) and NREM episode mean duration (right) comparing baseline to both Dex (25 and 50 μg/kg) and zolpidem. *C*, *Vgat-shRNA-Scr-LPO* mice BL states distribution as percentage of 1 h in Wake (left), NREM (center) and REM sleep (right) compared with the distribution after injection at ZT21 of Dex 25 μg/kg (red), Dex 50 μg/kg (green) and zolpidem 5 mg/kg (blue) at ZT21. *D*, Control *Vgat-shRNA-Scr-LPO* number of NREM sleep episodes (left) and NREM sleep episode mean duration (right) comparing BL to Dex (25 μg/kg and 50 μg/kg) and to zolpidem (5 mg/kg). For panels *A*, *B*, *Vgat shRNA-GluN1-LPO*, $n = 4$. For panels *C*, *D*, *Vgat-shRNA-scr-LPO*, $n = 6$. Data in all panels are represented as mean ± SEM (*$p < 0.05$, **$p < 0.005$).

The sleep homeostasis process is reflected in changes in EEG δ power (Borbély et al., 2016). During the 24-h cycle, δ power is highest during the "lights on" sleep phase and declines as each NREM sleep bout progresses (Fig. 6*D*,*E*), which is thought to reflect the dissipation of the homeostatic sleep drive (Borbély et al., 2016). After SD, neocortical activity in the subsequent ("recovery") NREM sleep is deeper (more synchronized and thus has a higher δ power). However, we found that NMDA receptor deletion in LPO did not affect sleep homeostasis as defined by the classical criteria, EEG δ power showed its usual variation, an increase and decrease over 24 h. Even placing $\Delta GluN1$-LPO mice under high sleep pressure by SD did not enable the mice to sleep well. The sleep fragmentation persisted even during the recovery sleep, and the fragmented sleep started with a higher δ power, as expected for recovery sleep in the sleep homeostasis model. So, the sleep homeostatic process seems independent of the mechanism maintaining consolidated sleep. In fact, during SD, $\Delta GluN1$-LPO mice made multiple attempted entries to sleep. It was as if the mice were chronically sleepy, but they nonetheless were not driven to sleep.

Many people suffer from occasional insomnia, but it can become a debilitating condition (Roth et al., 2011). Insomnia, as a clinical disorder, is defined as an inability to initiate or maintain sleep at least three times a week over three months, even when sleep conditions are otherwise optimal (Van Someren, 2020). Insomniacs frequently report that their sleep is nonrestorative and that they sleep less. In fact, insomnia sufferers often have the same amounts of EEG-defined NREM sleep as controls, but oscillate frequently between wake and NREM sleep, so that

their sleep is fragmented (Van Someren, 2020). The *Vgat-shRNA-GluN1-LPO* mice, which have the same amount of sleep, but high sleep-wake fragmentation, could be a useful model for intractable insomnia.

Behavioral therapy is often ineffective for treating intractable insomnia disorder, and medication remains an alternative approach if used cautiously (Shahid et al., 2012; An et al., 2020; Van Someren, 2020). Unlike SD, which is usually efficient at inducing sleep, drugs could treat quite effectively the insomnia of $\Delta GluN1$-LPO mice. Dex could transiently restore consolidated NREM sleep. Dex, an $\alpha 2$ adrenergic agonist, induces stage 3 NREM sleep in humans and NREM-like sleep in animals (Gelegen et al., 2014; Zhang et al., 2015; Akeju et al., 2018), and requires galanin/GABA neurons in LPO for its effects (Ma et al., 2019). Zolpidem (Ambien), a GABA$_A$ receptor positive modulator, is a widely prescribed sleeping medication (Wisden et al., 2019). Its main effect in humans is to reduce latency to NREM sleep rather than maintaining consolidated sleep. Nevertheless, zolpidem did have a beneficial effect on both $\Delta GluN1$-LPO and *Vgat-shRNA-GluN1-LPO* mice, restoring longer periods of NREM sleep.

Our findings also demonstrate a new aspect of REM sleep generation. REM sleep is characterized by a high $\theta:\delta$ frequency ratio in the EEG together with muscle atonia. In rodents, the θ itself detected in the cortical EEG seems to originate mostly from the hippocampus. Indeed, the θ activation during REM is required for memory processing (Boyce et al., 2016; Izawa et al., 2019). Although the brainstem circuitry that generates muscle atonia during REM sleep is reasonably

well understood, the circuitry that produces the θ activity in the EEG during REM sleep is only partially characterized, seeming to require distributed circuitry throughout the forebrain (Renouard et al., 2015; Peever and Fuller, 2016; Luppi et al., 2017; Izawa et al., 2019; Yamada and Ueda, 2019), including the MCH NREM-REM-promoting neurons in the lateral hypothalamus (Jego et al., 2013), REM-off and REM-on neurons in the dorsal medial hypothalamus (K.S. Chen et al., 2018), and GABA and cholinergic neurons in the medial septum that project to the hippocampus (Yoder and Pang, 2005). Although LPO is known to be required for REM sleep (Lu et al., 2000, 2002), we were surprised to discover that LPO neurons, regardless of type (e.g., *galanin*, *Vgat*, *Vglut2*), have actually their highest activity during REM sleep. We found that GluN1 knock-down in GABA and Vglut2 cells of LPO did not influence REM sleep, whereas the pan knock-out in all LPO neurons did, so the cell type(s) expressing NMDA receptors responsible for REM sleep generation in LPO require further investigation.

We speculate that NMDA receptor properties could be responsible for maintaining NREM and REM sleep promoting LPO neurons in the "on" state. In contrast to AMPA-gated ionotropic glutamate receptors, NMDA receptors stay open for around 100 ms to 1 s, as well as having a voltage-dependent magnesium block (Paoletti et al., 2013). Because of these properties, NMDA receptors have been intensely studied for their role in synaptic plasticity. But these same properties also allow NMDA receptors to act as pacemakers, controlling rhythmic firing, e.g., in those circuits involved in breathing, swimming, and walking (Steenland et al., 2008; Li et al., 2010), as well as contributing to the generation of burst firing of reticular thalamic neurons (Deleuze and Huguenard, 2016). The long open times of NMDA receptors, especially those located extrasynaptically, could be contributing to tonic excitation (Sah et al., 1989; Neupane et al., 2021), stabilizing hypothalamic sleep-on neurons in their firing mode. It will be interesting to see whether this role of NMDA receptors generalizes to other sleep-promoting circuits. For example, we previously found that genetic silencing of mouse lateral habenula neurons with tetanus toxin light-chain produced high NREM sleep-wake fragmentation with conserved amounts of total sleep and wake (Gelegen et al., 2018). It seems likely that disrupting NMDA receptors on these cells would also produce insomnia, given that that NMDA receptors are needed to keep lateral habenula cells in burst firing (active) mode (Yang et al., 2018; Cui et al., 2019).

In conclusion, we have found that selectively reducing NMDA receptors in the LPO hypothalamic area causes insomnia (Wake-NREM sleep fragmentation) and loss of θ activity during REM sleep. Given that sleep homeostasis is intact in mice with no NMDA receptors in LPO hypothalamus, the mechanism of sleep maintenance is distinct from that of the sleep drive itself.

References

Abraham NM, Egger V, Shimshek DR, Renden R, Fukunaga I, Sprengel R, Seeburg PH, Klugmann M, Margrie TW, Schaefer AT, Kuner T (2010) Synaptic inhibition in the olfactory bulb accelerates odor discrimination in mice. Neuron 65:399–411.

Adams R, Brown GT, Davidson M, Fisher E, Mathisen J, Thomson G, Webster NR (2013) Efficacy of dexmedetomidine compared with midazolam for sedation in adult intensive care patients: a systematic review. Br J Anaesth 111:703–710.

Akeju O, Hobbs LE, Gao L, Burns SM, Pavone KJ, Plummer GS, Walsh EC, Houle TT, Kim SE, Bianchi MT, Ellenbogen JM, Brown EN (2018) Dexmedetomidine promotes biomimetic non-rapid eye movement stage 3 sleep in humans: a pilot study. Clin Neurophysiol 129:69–78.

An JX, Williams JP, Fang QW, Wang Y, Liu H, Shi L, Zhang WH (2020) Feasibility of patient-controlled sleep with dexmedetomidine in treating chronic intractable insomnia. Nat Sci Sleep 12:1033–1042.

Anisimov VN, Herbst JA, Abramchuk AN, Latanov AV, Hahnloser RH, Vyssotski AL (2014) Reconstruction of vocal interactions in a group of small songbirds. Nat Methods 11:1135–1137.

Ariño H, Muñoz-Lopetegi A, Martinez-Hernandez E, Armangue T, Rosa-Justicia M, Escudero D, Matos N, Graus F, Sugranyes G, Castro-Fornieles J, Compte A, Dalmau J, Santamaria J (2020) Sleep disorders in anti-NMDAR encephalitis. Neurology 95:e671–e684.

Borbély AA, Daan S, Wirz-Justice A, Deboer T (2016) The two-process model of sleep regulation: a reappraisal. J Sleep Res 25:131–143.

Boyce R, Glasgow SD, Williams S, Adamantidis A (2016) Causal evidence for the role of REM sleep theta rhythm in contextual memory consolidation. Science 352:812–816.

Brüning F, Noya SB, Bange T, Koutsouli S, Rudolph JD, Tyagarajan SK, Cox J, Mann M, Brown SA, Robles MS (2019) Sleep-wake cycles drive daily dynamics of synaptic phosphorylation. Science 366:eaav3617.

Burgdorf JS, Vitaterna MH, Olker CJ, Song EJ, Christian EP, Sorensen L, Turek FW, Madsen TM, Khan MA, Kroes RA, Moskal JR (2019) NMDAR activation regulates the daily rhythms of sleep and mood. Sleep 42:zsz135.

Chen TW, Wardill TJ, Sun Y, Pulver SR, Renninger SL, Baohan A, Schreiter ER, Kerr RA, Orger MB, Jayaraman V, Looger LL, Svoboda K, Kim DS (2013) Ultrasensitive fluorescent proteins for imaging neuronal activity. Nature 499:295–300.

Chen KS, Xu M, Zhang Z, Chang WC, Gaj T, Schaffer DV, Dan Y (2018) A hypothalamic switch for REM and non-REM sleep. Neuron 97:1168–1176.e4.

Chung S, Weber F, Zhong P, Tan CL, Nguyen TN, Beier KT, Hörmann N, Chang WC, Zhang Z, Do JP, Yao S, Krashes MJ, Tasic B, Cetin A, Zeng H, Knight ZA, Luo L, Dan Y (2017) Identification of preoptic sleep neurons using retrograde labelling and gene profiling. Nature 545:477–481.

Cui Y, Hu S, Hu H (2019) Lateral habenular burst firing as a target of the rapid antidepressant effects of ketamine. Trends Neurosci 42:179–191.

Dalmau J, Armangué T, Planagumà J, Radosevic M, Mannara F, Leypoldt F, Geis C, Lancaster E, Titulaer MJ, Rosenfeld MR, Graus F (2019) An update on anti-NMDA receptor encephalitis for neurologists and psychiatrists: mechanisms and models. Lancet Neurol 18:1045–1057.

Deboer T (2018) Sleep homeostasis and the circadian clock: do the circadian pacemaker and the sleep homeostat influence each other's functioning? Neurobiol Sleep Circadian Rhythms 5:68–77.

Deleuze C, Huguenard JR (2016) Two classes of excitatory synaptic responses in rat thalamic reticular neurons. J Neurophysiol 116:995–1011.

Donlea JM, Alam MN, Szymusiak R (2017) Neuronal substrates of sleep homeostasis; lessons from flies, rats and mice. Curr Opin Neurobiol 44:228–235.

Franken P (2013) A role for clock genes in sleep homeostasis. Curr Opin Neurobiol 23:864–872.

Funato H, et al. (2016) Forward-genetics analysis of sleep in randomly mutagenized mice. Nature 539:378–383.

Gelegen C, Gent TC, Ferretti V, Zhang Z, Yustos R, Lan F, Yang Q, Overington DW, Vyssotski AL, van Lith HA, Wisden W, Franks NP (2014) Staying awake–a genetic region that hinders α2 adrenergic receptor agonist-induced sleep. Eur J Neurosci 40:2311–2319.

Gelegen C, Miracca G, Ran MZZ, Harding EC, Ye ZW, Yu X, Tossell K, Houston CM, Yustos R, Hawkins ED, Vyssotski AL, Dong HLL, Wisden W, Franks NP (2018) Excitatory pathways from the lateral habenula enable propofol-induced sedation. Curr Biol 28:580–587.e5.

Greene RW, Bjorness TE, Suzuki A (2017) The adenosine-mediated, neuronal-glial, homeostatic sleep response. Curr Opin Neurobiol 44:236–242.

Hanlon EC, Vyazovskiy VV, Faraguna U, Tononi G, Cirelli C (2011) Synaptic potentiation and sleep need: clues from molecular and electrophysiological studies. Curr Top Med Chem 11:2472–2482.

Honda T, Fujiyama T, Miyoshi C, Ikkyu A, Hotta-Hirashima N, Kanno S, Mizuno S, Sugiyama F, Takahashi S, Funato H, Yanagisawa M (2018) A single phosphorylation site of SIK3 regulates daily sleep amounts and sleep need in mice. Proc Natl Acad Sci U S A 115:10458–10463.

Izawa S, Chowdhury S, Miyazaki T, Mukai Y, Ono D, Inoue R, Ohmura Y, Mizoguchi H, Kimura K, Yoshioka M, Terao A, Kilduff TS, Yamanaka A (2019) REM sleep-active MCH neurons are involved in forgetting hippocampus-dependent memories. Science 365:1308–1313.

Jego S, Glasgow SD, Herrera CG, Ekstrand M, Reed SJ, Boyce R, Friedman J, Burdakov D, Adamantidis AR (2013) Optogenetic identification of a rapid eye movement sleep modulatory circuit in the hypothalamus. Nat Neurosci 16:1637–1643.

John J, Kumar VM (1998) Effect of NMDA lesion of the medial preoptic neurons on sleep and other functions. Sleep 21:587–598.

Klugmann M, Symes CW, Leichtlein CB, Klaussner BK, Dunning J, Fong D, Young D, During MJ (2005) AAV-mediated hippocampal expression of short and long Homer 1 proteins differentially affect cognition and seizure activity in adult rats. Mol Cell Neurosci 28:347–360.

Krashes MJ, Koda S, Ye C, Rogan SC, Adams AC, Cusher DS, Maratos-Flier E, Roth BL, Lowell BB (2011) Rapid, reversible activation of AgRP neurons drives feeding behavior in mice. J Clin Invest 121:1424–1428.

Kroeger D, Absi G, Gagliardi C, Bandaru SS, Madara JC, Ferrari LL, Arrigoni E, Münzberg H, Scammell TE, Saper CB, Vetrivelan R (2018) Galanin neurons in the ventrolateral preoptic area promote sleep and heat loss in mice. Nat Commun 9:4129.

Laurie DJ, Seeburg PH (1994) Regional and developmental heterogeneity in splicing of the rat brain NMDAR1 mRNA. J Neurosci 14:3180–3194.

Leshan RL, Greenwald-Yarnell M, Patterson CM, Gonzalez IE, Myers MG Jr (2012) Leptin action through hypothalamic nitric oxide synthase-1-expressing neurons controls energy balance. Nat Med 18:820–823.

Li WC, Roberts A, Soffe SR (2010) Specific brainstem neurons switch each other into pacemaker mode to drive movement by activating NMDA receptors. J Neurosci 30:16609–16620.

Liu S, Liu Q, Tabuchi M, Wu MN (2016) Sleep drive is encoded by neural plastic changes in a dedicated circuit. Cell 165:1347–1360.

Lu J, Greco MA, Shiromani P, Saper CB (2000) Effect of lesions of the ventrolateral preoptic nucleus on NREM and REM sleep. J Neurosci 20:3830–3842.

Lu J, Bjorkum AA, Xu M, Gaus SE, Shiromani PJ, Saper CB (2002) Selective activation of the extended ventrolateral preoptic nucleus during rapid eye movement sleep. J Neurosci 22:4568–4576.

Luppi PH, Billwiller F, Fort P (2017) Selective activation of a few limbic structures during paradoxical (REM) sleep by the claustrum and the supramammillary nucleus: evidence and function. Curr Opin Neurobiol 44:59–64.

Ma Y, Miracca G, Yu X, Harding EC, Miao A, Yustos R, Vyssotski AL, Franks NP, Wisden W (2019) Galanin neurons unite sleep homeostasis and α2-adrenergic sedation. Curr Biol 29:3315–3322.e3.

McGinty DJ, Sterman MB (1968) Sleep suppression after basal forebrain lesions in the cat. Science 160:1253–1255.

Monyer H, Sprengel R, Schoepfer R, Herb A, Higuchi M, Lomeli H, Burnashev N, Sakmann B, Seeburg PH (1992) Heteromeric NMDA receptors: molecular and functional distinction of subtypes. Science 256:1217–1221.

Monyer H, Burnashev N, Laurie DJ, Sakmann B, Seeburg PH (1994) Developmental and regional expression in the rat brain and functional properties of four NMDA receptors. Neuron 12:529–540.

Moriyoshi K, Masu M, Ishii T, Shigemoto R, Mizuno N, Nakanishi S (1991) Molecular cloning and characterization of the rat NMDA receptor. Nature 354:31–37.

Nauta WJ (1946) Hypothalamic regulation of sleep in rats; an experimental study. J Neurophysiol 9:285–316.

Neupane C, Sharma R, Pai YH, Lee SY, Jeon BH, Kim HW, Stern JE, Park JB (2021) High salt intake recruits tonic activation of NR2D subunit-containing extrasynaptic NMDARs in vasopressin neurons. J Neurosci 41:1145–1156.

Niwa Y, Kanda GN, Yamada RG, Shi S, Sunagawa GA, Ukai-Tadenuma M, Fujishima H, Matsumoto N, Masumoto KH, Nagano M, Kasukawa T, Galloway J, Perrin D, Shigeyoshi Y, Ukai H, Kiyonari H, Sumiyama K, Ueda HR (2018) Muscarinic acetylcholine receptors Chrm1 and Chrm3 are essential for REM sleep. Cell Rep 24:2231–2247.e7.

Paoletti P, Bellone C, Zhou Q (2013) NMDA receptor subunit diversity: impact on receptor properties, synaptic plasticity and disease. Nat Rev Neurosci 14:383–400.

Papouin T, Ladépêche L, Ruel J, Sacchi S, Labasque M, Hanini M, Groc L, Pollegioni L, Mothet JP, Oliet SH (2012) Synaptic and extrasynaptic NMDA receptors are gated by different endogenous coagonists. Cell 150:633–646.

Peever J, Fuller PM (2016) Neuroscience: a distributed neural network controls REM sleep. Curr Biol 26:R34–R35.

Raccuglia D, Huang S, Ender A, Heim MM, Laber D, Suarez-Grimalt R, Liotta A, Sigrist SJ, Geiger JRP, Owald D (2019) Network-specific synchronization of electrical slow-wave oscillations regulates sleep drive in Drosophila. Curr Biol 29:3611–3621.e3.

Reichert S, Pavón Arocas O, Rihel J (2019) The neuropeptide galanin is required for homeostatic rebound sleep following increased neuronal activity. Neuron 104:370–384.e5.

Renouard L, Billwiller F, Ogawa K, Clement O, Camargo N, Abdelkarim M, Gay N, Scote-Blachon C, Toure R, Libourel PA, Ravassard P, Salvert D, Peyron C, Claustrat B, Leger L, Salin P, Malleret G, Fort P, Luppi PH (2015) The supramammillary nucleus and the claustrum activate the cortex during REM sleep. Sci Adv 1:e1400177.

Roth T, Coulouvrat C, Hajak G, Lakoma MD, Sampson NA, Shahly V, Shillington AC, Stephenson JJ, Walsh JK, Kessler RC (2011) Prevalence and perceived health associated with insomnia based on DSM-IV-TR; International Statistical Classification of Diseases and Related Health Problems, Tenth Revision; and Research Diagnostic Criteria/International Classification of Sleep Disorders. Biol Psychiatry 69:592–600.

Sah P, Hestrin S, Nicoll RA (1989) Tonic activation of NMDA receptors by ambient glutamate enhances excitability of neurons. Science 246:815–818.

Schmidt EF, Kus L, Gong S, Heintz N (2013) BAC transgenic mice and the GENSAT database of engineered mouse strains. Cold Spring Harb Protoc 2013:pdb.top073692.

Shahid A, Chung SA, Phillipson R, Shapiro CM (2012) An approach to long-term sedative-hypnotic use. Nat Sci Sleep 4:53–61.

Sherin JE, Shiromani PJ, McCarley RW, Saper CB (1996) Activation of ventrolateral preoptic neurons during sleep. Science 271:216–219.

Steenland HW, Liu H, Horner RL (2008) Endogenous glutamatergic control of rhythmically active mammalian respiratory motoneurons in vivo. J Neurosci 28:6826–6835.

Stegmeier F, Hu G, Rickles RJ, Hannon GJ, Elledge SJ (2005) A lentiviral microRNA-based system for single-copy polymerase II-regulated RNA interference in mammalian cells. Proc Natl Acad Sci U S A 102:13212–13217.

Szymusiak R, Gvilia I, McGinty D (2007) Hypothalamic control of sleep. Sleep Med 8:291–301.

Tatsuki F, Sunagawa GA, Shi S, Susaki EA, Yukinaga H, Perrin D, Sumiyama K, Ukai-Tadenuma M, Fujishima H, Ohno R, Tone D, Ode KL, Matsumoto K, Ueda HR (2016) Involvement of Ca(2+)-dependent hyperpolarization in sleep duration in mammals. Neuron 90:70–85.

Tobler I, Deboer T, Fischer M (1997) Sleep and sleep regulation in normal and prion protein-deficient mice. J Neurosci 17:1869–1879.

Tomita J, Ueno T, Mitsuyoshi M, Kume S, Kume K (2015) The NMDA receptor promotes sleep in the fruit fly, Drosophila melanogaster. PLoS One 10:e0128101.

Tovar KR, McGinley MJ, Westbrook GL (2013) Triheteromeric NMDA receptors at hippocampal synapses. J Neurosci 33:9150–9160.

Tsien JZ, Huerta PT, Tonegawa S (1996) The essential role of hippocampal CA1 NMDA receptor-dependent synaptic plasticity in spatial memory. Cell 87:1327–1338.

Van Someren EJW (2020) Brain mechanisms of insomnia: new perspectives on causes and consequences. Physiol Rev 101:995–1046.

Vong L, Ye C, Yang Z, Choi B, Chua S Jr, Lowell BB (2011) Leptin action on GABAergic neurons prevents obesity and reduces inhibitory tone to POMC neurons. Neuron 71:142–154.

Vyssotski AL, Dell'Omo G, Dell'Ariccia G, Abramchuk AN, Serkov AN, Latanov AV, Loizzo A, Wolfer DP, Lipp HP (2009) EEG responses to visual landmarks in flying pigeons. Curr Biol 19:1159–1166.

Wang Z, et al. (2018) Quantitative phosphoproteomic analysis of the molecular substrates of sleep need. Nature 558:435–439.

Wisden W, Yu X, Franks NP (2019) GABA receptors and the pharmacology of sleep. Handb Exp Pharmacol 253:279–304.

Yamada RG, Ueda HR (2019) Molecular mechanisms of REM sleep. Front Neurosci 13:1402.

Yang Y, Cui YH, Sang KN, Dong YY, Ni ZY, Ma SS, Hu HL (2018) Ketamine blocks bursting in the lateral habenula to rapidly relieve depression. Nature 554:317–322.

Yoder RM, Pang KCH (2005) Involvement of GABAergic and cholinergic medial septal neurons in hippocampal theta rhythm. Hippocampus 15:381–392.

Yu X, Ye Z, Houston CM, Zecharia AY, Ma Y, Zhang Z, Uygun DS, Parker S, Vyssotski AL, Yustos R, Franks NP, Brickley SG, Wisden W (2015) Wakefulness is governed by GABA and histamine cotransmission. Neuron 87:164–178.

Zhang Z, Ferretti V, Güntan I, Moro A, Steinberg EA, Ye Z, Zecharia AY, Yu X, Vyssotski AL, Brickley SG, Yustos R, Pillidge ZE, Harding EC, Wisden W, Franks NP (2015) Neuronal ensembles sufficient for recovery sleep and the sedative actions of alpha2 adrenergic agonists. Nat Neurosci 18:553–561.